JGR Oceans

RESEARCH ARTICLE
10.1029/2024JC021886

Processes That Influence Bottom Temperatures in the California Current System

M. A. Alexander[1], J. D. Scott[1,2], M. G. Jacox[1,3,4], D. J. Amaya[1], and L. M. Wilczynski[5]

[1]NOAA/Physical Sciences Laboratory, Boulder, CO, USA, [2]University of Colorado/CIRES, Boulder, CO, USA, [3]NOAA/Southwest Fisheries Science Center, Monterey, CA, USA, [4]University of California Santa Cruz, Santa Cruz, CA, USA, [5]College of Earth, Ocean and Atmospheric Sciences, Oregon State University, Corvallis, OR, USA

Abstract Bottom water temperature (BWT) strongly influences marine organisms in coastal waters. Although subsurface observations are limited, the recent development of high-resolution reanalyses enables a detailed three-dimensional view of the ocean, including on the continental shelf. Here, we use the GLORYS 1/12° (~9 km) reanalysis during 1993–2019 to examine processes that influence BWT anomalies on the shelf (≤400 m bottom depth) off the West Coast of Baja California and the contiguous US. We examine the relationship between BWT anomalies and other ocean variables, including mixed layer depth (MLD), thermocline depth (TD), thermocline and bottom temperature gradients, and bottom currents. The strongest and most spatially coherent connections with BWT anomalies occur for MLD during winter and TD in summer. BWT anomalies are also correlated with the local sea surface height (SSH) anomalies with maxima at 2–5 days lag. On subseasonal timescales, the lag of the maximum coherence of SSH at the southern tip of Baja California with both SSH and BWT increases northwards, consistent with propagating coastally trapped waves (CTWs), although the BWT anomalies decrease with latitude. Like SST and SSH, BWT anomalies are coherent along the entire West Coast on interannual timescales, reflecting ENSO's influence on the northeast Pacific. In contrast to CTWs, wind-driven upwelling's impact on BWT anomalies increases with latitude. Regional ocean model experiments confirm the GLORYS analysis and highlight the importance of remote wind-driven effects, in addition to local winds, on BWT in the northern part of the domain.

Plain Language Summary Temperature strongly influences marine organisms through their metabolism, growth and behavior, including species that live on or near the bottom, such as shellfish, crabs, and flounder. Although there have been many studies documenting sea surface temperature variability, much less is known about bottom water temperatures due to a lack of observations. Here, we use a recently developed reanalysis, which combines a wide array of observations with a computer model to obtain a fine-scale view of the coastal ocean. We examine processes that influence bottom water temperature along the West Coast of the contiguous United States and Baja California, where the ocean depth is less than 400 m. The temperature near the bottom and at the surface often vary together, especially during winter where the ocean is shallow when storms vertically mix the upper ocean. Deeper in the ocean, vertical movement of the thermocline, where the temperature decreases rapidly with depth, can also generate large bottom water temperature anomalies. Bottom water temperatures are more strongly affected by winds off the Pacific Northwest US coast and ocean processes initiated in the tropics further south. ENSO events have a strong influence on bottom water temperatures in addition to those at the surface.

Key Points:

- A high-resolution reanalysis reveals ENSO's impact on bottom water temperature anomalies on the shelf in the California Current system
- Mixed layer and thermocline depth strongly influence bottom water temperature anomalies in winter and summer, respectively
- Bottom water temperatures are more strongly affected by winds in the north and poleward propagating coastally trapped waves in the south

Supporting Information:

Supporting Information may be found in the online version of this article.

Correspondence to:

M. A. Alexander,
michael.alexander@noaa.gov

Citation:

Alexander, M. A., Scott, J. D., Jacox, M. G., Amaya, D. J., & Wilczynski, L. M. (2025). Processes that influence bottom temperatures in the California Current system. *Journal of Geophysical Research: Oceans*, *130*, e2024JC021886. https://doi.org/10.1029/2024JC021886

Received 23 SEP 2024
Accepted 20 JAN 2025

Author Contributions:

Conceptualization: M. A. Alexander, J. D. Scott, M. G. Jacox, L. M. Wilczynski
Formal analysis: M. A. Alexander, J. D. Scott, M. G. Jacox
Funding acquisition: M. A. Alexander
Investigation: M. A. Alexander, J. D. Scott, M. G. Jacox, D. J. Amaya, L. M. Wilczynski
Methodology: M. A. Alexander, J. D. Scott, M. G. Jacox, D. J. Amaya
Project administration: M. A. Alexander
Resources: M. A. Alexander, M. G. Jacox
Software: J. D. Scott, M. G. Jacox
Supervision: M. A. Alexander
Validation: J. D. Scott, M. G. Jacox, D. J. Amaya

1. Introduction

Ocean temperature plays a critical role in the physical climate system and strongly influences chemical and biological processes. Given the relative abundance of data and archived model output, sea surface temperatures (SSTs) have been well studied relative to temperatures at depth, including bottom water temperatures (BWTs). Temperatures in coastal regions respond to a wide array of processes including vertical mixing, upwelling, coastally trapped waves (CTWs), regional currents and basin-scale phenomena especially the El Niño/Southern Oscillation (ENSO). However, the influence of these and other processes on BWT variability have been difficult to analyze in coastal regions due to sparse and inhomogeneous sampling, the importance of small-scale phenomena, and interactions with complex topography, including narrow shelves. Here, we explore processes that influence BWTs along the West Coast of the United States and Baja California using a recently developed high-resolution ocean reanalysis along with regional ocean model simulations.

Visualization: M. G. Jacox
Writing – original draft: M. A. Alexander
Writing – review & editing: M. A. Alexander, J. D. Scott, M. G. Jacox, D. J. Amaya, L. M. Wilczynski

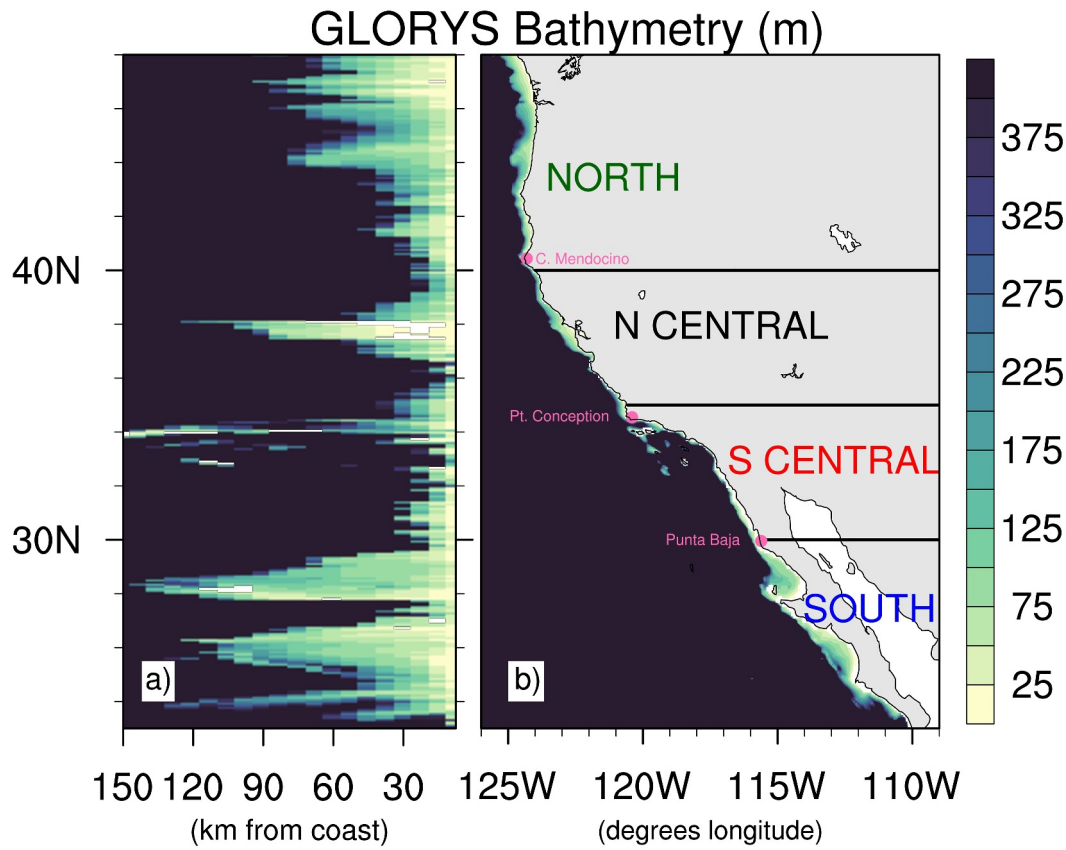

Figure 1. Depth of the ocean's bottom in the CCS domain. GLORYS bathymetry (m) on the shelf off the West Coast of Baja California and the contiguous US, approximately 23°–50°N. (a) The bottom depth on the shelf (<400 m) on the model grid as a function of latitude and distance from the coastline and (b) in a traditional map view for the north (N), north central (NC), south central (SC), and south (S) regions. Half of the latitudes have a shelf width between 21 and 58 km.

BWT variations can influence benthic and demersal species in myriad ways, including physiological processes, habitat range, recruitment, and ecological interactions. For example, along the North American West Coast, the development and survival of juvenile Dungeness crab, a highly valuable commercial species, are adversely affected by high temperatures during summer (Sulkin et al., 1996). Using bioenergetic models, Harvey (2009) found that the growth, maturation, and prey consumption of three species of California Current Large Marine Ecosystem groundfish responded strongly to an increase in temperature. Temperature and vertical stratification can influence demersal fish via their effects on oxygen levels (Keller et al., 2015). Further, high temperatures increase the metabolic rate of ectothermic (cold-blooded) animals. By enhancing the metabolic rate, a bottom marine heatwave (Amaya, Alexander, Jacox, Scott, et al., 2023) in the Bering Sea contributed to the starvation of snow crabs beginning in 2018, crippling a $100 M/yr fishery (Szuwalksi et al., 2023). Similar events in the future could lead to the reduction and/or redistribution of suitable habitat for marine species on the northeast and West Coast US shelves (Slesinger et al., 2024). In addition, Morley et al. (2018) projected northward shifts of many species on the North American continental shelf due to warming associated with an increase in greenhouse gasses with some of the largest changes occurring for bottom-dwelling species along the US West Coast.

Multiple processes are influenced by the complex geologic features, including bays, canyons, channels, islands/seamounts, points, and volcanic ridges along the US West Coast and Baja California. The shelf is narrow, generally less than 150 km wide, and narrower than 60 km along most of the coast between 30°N and 43°N (Figure 1). It is somewhat wider west of Baja California Sur, including near 24°N and in San Juanico and Sebastián Vizcaíno bays, located at approximately 25°–26.25°N and 28°–29°N, respectively.

The bathymetry strongly affects the conditions on the shelf including BWTs. For example, vertical mixing by winds and buoyancy forcing links anomalies at the surface with those at depth and can link SST with BWT

anomalies depending on the depth of the mixed layer relative to the bathymetric depth (Alexander et al., 2023; Amaya, Alexander, Jacox, Scott, et al., 2023). Wind-driven off-shore Ekman transport, partly compensated by geostrophic currents (Jacox et al., 2018), leads to upwelling of cold nutrient-rich water to the surface layer. The wind-driven changes in the vertical velocity can also displace the thermocline (Bindoff & Mcdougall, 1994). In the eastern North Pacific, Kelvin and other CTWs propagate poleward, causing changes in SSH and thermocline depth as well as anomalous alongshore currents. These CTWs can be generated locally by the wind or generated remotely and subsequently propagate into the region (Clarke, 1977; Enfield & Allen, 1983; Frischknecht et al., 2015; Hughes et al., 2019; Pierce et al., 2000). Coastal conditions are also influenced by the complex California Current, which generally has southward flow near the surface and a northward undercurrent at depth but varies with latitude and season (Checkley & Barth, 2009; Hickey, 1979, 1998; Thomson & Krassovski, 2010). In addition to the main off-shore branch, the CCS includes a strong equatorward coastal jet (Barth et al., 2000), which influences the shallow portions of the shelf, while below the thermocline, relatively deep portions of the shelf are affected by the undercurrent (Marchesiello et al., 2003). Fluctuations in the California Current System can also influence temperature anomalies along the West Coast (Kurczyn et al., 2019; Ray et al., 2020).

ENSO strongly affects the eastern North Pacific through both the atmosphere and the ocean. ENSO teleconnections influence much of the North Pacific via the "atmospheric bridge," where changes in the wind and air temperature result in surface heat flux, entrainment and Ekman ocean transport anomalies that result in ocean temperature anomalies (e.g., Alexander et al., 2002). In addition, ENSO-driven changes in winds along the West Coast of North America affect upwelling and thus near-shore ocean temperatures (Jacox, Alexander, et al., 2019). Oceanic Kelvin waves, a key component of ENSO events, propagate along the equator and then poleward upon reaching the coast. These CTWs propagate along the entire West Coast of North America and can even reach the Gulf of Alaska several months after departing the tropics, although their influence on the ocean decreases with latitude as they are dissipated and zonal width decreases in contrast to wind forcing which becomes more important at higher latitudes (Amaya et al., 2022; Enfield & Allen, 1980; Frischknecht et al., 2015; Gómez-Valdivia et al., 2017; Hermann et al., 2009; Pares-Sierra & O'Brien, 1989). In addition to ENSO, other phenomena influence the evolution of temperature anomalies along the West Coast of North America, such that warm (cold) events in the CCS can occur independent of El Niño (La Niña) events (Fiedler & Mantua, 2017). During most El Niño events SSHs increase, the thermocline deepens and anomalous poleward currents develop along the North American coast (Lynn & Bograd, 2002; Lynn et al., 1995). Indeed, SSH anomalies produced by strong El Niño events contributed to marine heatwaves (MHWs) on the nearshore seabeds of North America in 1997–1998 and 2013–2015 (Amaya, Alexander, Jacox, Scott, et al., 2023). During these events, BWT anomalies west of Baja California reached 5°C, exceeding the SST anomalies in the same location.

In addition to ENSO, other phenomena influence the evolution of temperature anomalies along the West Coast of North America. For example, the formation of the extreme MHW in the eastern North Pacific beginning in 2013, that is, "the Blob" (e.g., Bond et al., 2015) predated the 2015–2016 ENSO event and contributed to warming in nearshore waters along Washington's Olympic coast (Koehlinger et al., 2023). In addition, Koehlinger et al. found that short-term warm events that extend over the water column can occur in the absence of a large-scale marine heatwave due to downwelling-favorable winds.

Although many studies have investigated the impact of ENSO, the Pacific Decadal Oscillation (PDO, Mantua et al., 1997) and North Pacific Gyre Oscillation (NPGO; Di Lorenzo et al., 2008) on SSTs and oceanic conditions along the North American coast, there has been little analysis of their influence on bottom temperature. In addition, the studies that have examined the prediction of BWTs along the West Coast did not focus on the mechanisms that caused them. To obtain a reasonable representation of the bathymetry and coastal oceanography, we use a recently developed high-resolution ocean reanalysis along with regional ocean model simulations to examine the relationship between SST and BWT anomalies. We then examine the different processes that influence BWTs along the West Coast, including their variation with latitude and season and their relationship to ENSO.

2. Ocean Reanalysis and Regional Ocean Model Simulations

2.1. GLORYS Reanalysis

Ocean fields, including temperatures and currents, were obtained from the Global Ocean/Ice Reanalysis and Simulations (GLORYS, Lellouche et al., 2021), which combines a dynamic ocean model with observations from

several different sources. GLORYS uses the Nucleus for European Modeling of the Ocean (NEMO) platform (Madec, & The NEMO Team, 2008), driven by surface fluxes from the European Center for Medium-Range Weather Forecasts (ECMWF) ERA-Interim atmospheric reanalysis (Dee et al., 2011). Along-track satellite altimetry for the SSH, satellite-based SST, sea ice concentrations, and in situ profiles of temperature and salinity, including ARGO floats, from the Coriolis Ocean database ReAnalysis (CORA) data set (Szekely et al., 2019) are inputs to the model assimilation system. Ocean observations are assimilated through a reduced-order Kalman filter. A 3D-VAR scheme is applied to correct for slowly evolving large-scale biases in temperature and salinity.

GLORYS output fields are archived daily from 1993 to 2019 on a 1/12° grid (∼9 km horizontal resolution in midlatitudes). The reanalysis has 50 vertical levels, with 22 levels in the upper 100 m. The near-surface layers have a vertical resolution of 1 m, with the layer thickness increasing with depth, reaching 450 m at 5,000 m. At this horizontal and vertical resolution, the model is able to represent the general characteristics of the shelf along the West Coast of North America but not the detailed structure of small bathymetric features (Figure 1). Still, several studies have shown that GLORYS compares well to independent (i.e., unassimilated) in situ measurements of nearshore ocean temperature throughout the CCS (Amaya, Alexander, Jacox, & Scott, 2023; Amaya, Alexander, Jacox, Scott, et al., 2023) and in other regions (Castillo-Trujillo et al., 2023).

Bottom water temperatures, and the process-based variables they may be influenced by, are obtained as follows. BWTs were obtained from the GLORYS archive. Values on the shelf are from areas where the bottom is shallower than 400 m. Mixed layer depth (MLD) is computed as the depth at which the water is 0.125 kg m^{-3} denser than the surface (without a minimum value constraint). This criterion was used by Monterey and Levitus (1997), Alexander et al. (2018), and Buckley et al. (2019) but is larger than the density difference used in some studies (e.g., Cai et al., 2021; de Boyer Montégut et al., 2004) and the MLD values provided by GLORYS. We chose to calculate MLD using the larger density jump, which reduces large daily MLD fluctuations and is more representative of the seasonal evolution of the MLD. The vertical temperature gradient at the bottom (∇T_{Bot}) is calculated from the two lowest model layers above the sea floor. The thermocline depth and strength are estimated using the variable representative isotherm (VRI) method, which Fiedler (2010) found to be the best of the several considered in the Pacific. In the VRI method, the thermocline temperature is given by $T_{\mathrm{MLD}} - 0.25^{*}(T_{\mathrm{MLD}} - T_{400\mathrm{m}})$, the thermocline depth (TD) is the depth at which this temperature occurs, and $T_{400\mathrm{m}}$ is obtained from the nearest point deeper than 400 m. The thermocline gradient (∇T_{Thrm}) is given by the difference in temperature between the MLD and TD divided by their difference in depth. If the temperature in the column never reaches that midpoint temperature, then TD and ∇T_{Thrm} are undefined, which occur when the MLD extends to the bottom. These quantities were computed daily and then averaged during winter (January–February–March, JFM) and summer (July–August–September, JAS). During winter, MLDs are less than ∼100 m over the entire domain and ∼60 m on the shelf, while in summer they are generally less than 20 m (Figure S1 in Supporting Information S1). The seasonal mean TD and its largest variability tend to occur in the upper half of the thermocline (Figures S2–S5 in Supporting Information S1).

Given that there are regional differences in the physics and ecology of the CCS, we examine area averages for north (N), north central (NC), south central (SC) and southern (S) regions, with divisions at 40°N, 35°N, and 30°N (Figure 1b), near Cape Mendocino, Point Conception, and Punta Baja, respectively. The northern three regions correspond with distinct meteorological and oceanographic regimes off the Oregon/Washington, Central/Northern California, and Southern California coasts (Dorman & Winant, 1995) and have been used in previous studies (e.g., Jacox, Alexander, et al., 2019). The division line at 30°N approximates the southern limit of the Southern California Bight and also corresponds to the southern boundary of the Regional Ocean Modeling System (ROMS) model domain used in our analysis (Section 2.2).

Heat budgets, a logical approach to examine the processes that govern BWT variability, are not possible here because: (a) data assimilation disrupts the conservation of properties including heat and momentum; (b) GLORYS output has been interpolated from an irregular to a uniform grid; (c) the variables are not archived at a sufficient frequency to accurately calculate nonlinear budget terms and (d) fields such as vertical velocity are extremely noisy especially in coastal regions. Instead, we will explore relationships between ocean variables and BWT anomalies using statistical methods.

2.2. Regional Ocean Model Simulations

In addition to the GLORYS reanalysis, we leverage regional ocean model simulations to further investigate drivers of bottom temperature variability. The ROMS simulations are configured for a U.S. West Coast domain spanning 30–48°N and offshore to 134°W with 1/10° horizontal resolution and 42 terrain-following vertical levels (Veneziani et al., 2009). Model forcing is derived from the Simple Ocean Data Assimilation reanalysis (Carton & Giese, 2008) for ocean boundary conditions with atmospheric forcing from a combination of Cross-Calibrated Multi-Platform winds (Atlas et al., 2011) and European Center for Medium-Range Weather Forecasting (ECMWF) ERA-40 and ERA-Interim atmospheric reanalyses (Dee et al., 2011; Uppala et al., 2005). Based on this configuration, a set of sensitivity experiments was performed to isolate the influences of forcing through the ocean and atmospheric boundaries (Section 3.4). These simulations are described in detail by Jacox et al. (2015); in brief, the simulation with fully realistic forcing (Control run) is complemented by one with realistic winds but climatological ocean boundary conditions (the "Wind" run) and another with realistic ocean boundary conditions but climatological winds (the "Ocean" run).

3. Results

3.1. SST and BWT

Time series of monthly SST and BWT anomalies averaged over the four coastal regions (N, NC, SC, S; see Figure 1) exhibit variability on a wide range of timescales (Figure 2). In general, the surface and bottom temperature anomalies vary contemporaneously in all four regions. However, they do differ at times, for example, between 2003 and 2007. The regional average correlation between SST and BWT anomalies ranges from 0.59 in NC, to 0.66 in N and SC, to 0.72 in S indicating that one can explain approximately ⅓ to ½ of the variance in the other. The SST and BWT anomalies are well correlated with each other even at individual grid points in both winter and summer except for deeper portions of *N* in summer (Figure S6 in Supporting Information S1). Since temperature anomalies extend over the depth of the mixed layer, SST and BWT anomalies become more synchronous as the MLD approaches the bottom (Alexander et al., 2023; Amaya, Alexander, Jacox, Scott, et al., 2023 and discussed further in Section 3.2).

The SSTs appear to exhibit more multiannual variability than BWTs albeit over a relatively short period of record. The BWT anomalies in the southern domain exhibit very strong interannual variability. Indeed, the BWT standard deviation ($\boldsymbol{\sigma}$) >1.5°C within ∼100 km of shore along wide portions of the shelf at approximately 26° and 28°N during both winter and summer with some locations exceeding 2.0°C (Figure 3). However, the variability is low for offshore locations at 24°N. The BWT $\boldsymbol{\sigma}$ is lower north of 30°N, ranging from approximately 0.4–1.2°C in both JFM and JAS, with lower values (<0.5°C) poleward of 38°N in summer.

The SST and BWT in all four regions exhibit anomalous warming associated with the 1997–1998 and 2015–2016 El Niño events (Figure 2, also see Amaya, Alexander, Jacox, Scott, et al., 2023). However, the anomalies are much larger at the bottom than at the surface during the 1997–1998 event with values exceeding 4.0°C in the southern region. Anomalous warming also occurred in the year prior to the second El Niño event, likely associated with "the Blob," an intense marine heatwave in the northeast Pacific, which started off-shore near the end of 2013 and spread over much of the northeast Pacific by early 2016 (e.g., Bond et al., 2015; Jacox, Tommasi, et al., 2019). The CCS exhibited positive SST anomalies beginning in early 2014 and remained above average through much of 2016 (Figure 2; Di Lorenzo & Mantua, 2016; Gentemann et al., 2017). The BWT anomalies exhibit two distinct peaks: one in 2014 and the second from late 2015 to early 2016. The first peak may reflect the influence of the weak/aborted 2014–2015 El Niño event. After the first peak, rapid cooling in the spring of 2015 was associated with anomalously strong coastal upwelling (Peterson et al., 2017). The cooling was confined to a narrow coastal band and is therefore reflected in BWT based on the near-shore area where the bottom is less than 400 m deep but not in the broader regional SST average. The influence of ENSO on BWTs along the West Coast is examined in greater detail in Section 3.3.2.

There is relatively strong coherence between regions for both SST and BWT anomalies; the highest anomaly correlation coefficients (ACC) occur for adjoining regions and are also slightly higher for BWT than SST anomalies (Figure 2c). For example, the ACCs for BWTs (SSTs) are 0.90 (0.85), 0.82 (0.75), and 0.68 (0.52) between the S and the SC, NC, and N regions, respectively (Figure 2c). The high correlations likely reflect large-scale processes that influence the CCS associated with ENSO and other large-scale phenomena (e.g., Chhak & Di

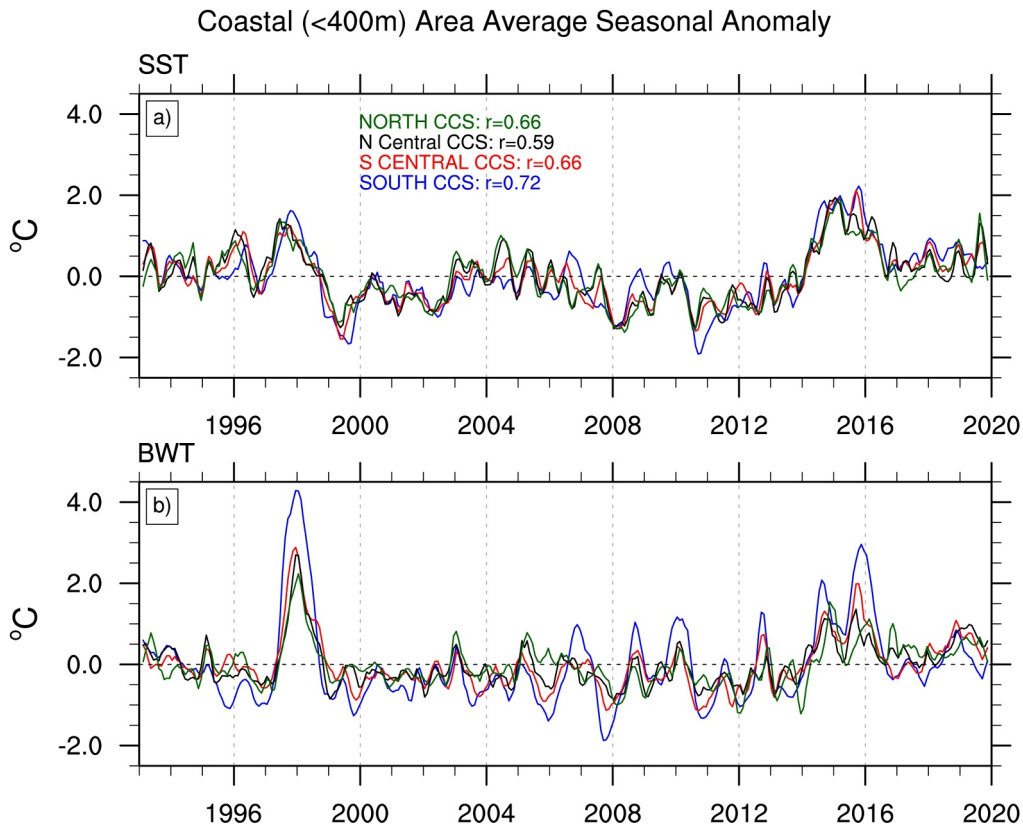

c) Regional ACC of seasonal SST and BWT

Region	S	SC	NC	N
N	0.52	0.66	0.74	
NC	0.72	0.85		0.83
SC	0.85		0.88	0.73
S		0.9	0.82	0.68

Figure 2. Time series of SST and BWT anomalies in the four CCS regions and the correlations between regions for each variable separately. Area average of the 3 month running mean of the (a) SST and (b) BWT anomalies (°C) on the continental shelf (<400 m deep) for the N (green), NC (black), SC (red), and south (blue) regions. The correlation between monthly SST and BWT anomalies in each of the four regions is given in (a). (c) Anomaly correlations between regions for SST (red, upper left) and BWT (blue lower right).

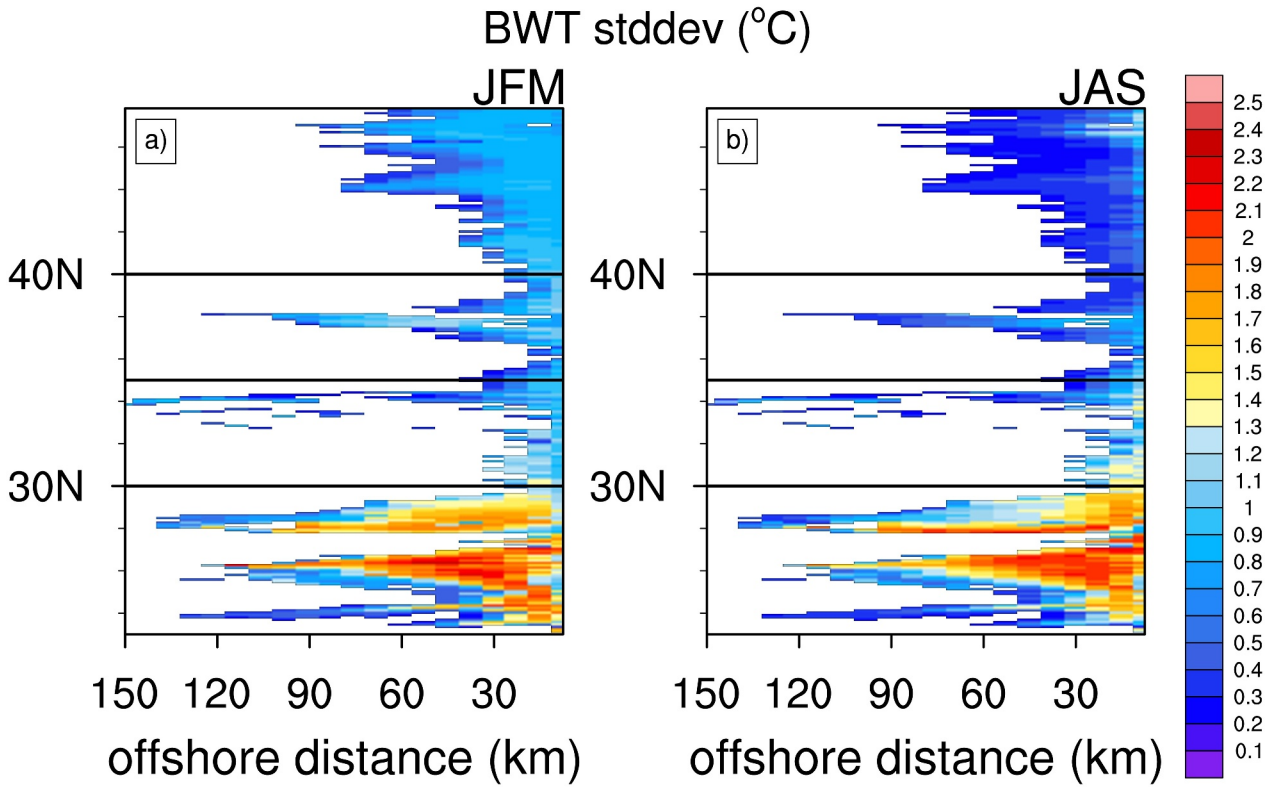

Figure 3. Interannual standard deviation (**σ**) of BWT (°C) on the continental shelf for (a) JFM and (b) JAS.

Lorenzo, 2007; Di Lorenzo et al., 2008; Liu & Alexander, 2007) but with some variations along the coast of North America, as discussed further in Section 3.3.

3.2. Local Vertical and Horizontal Processes

Multiple processes can influence BWT anomalies, including vertical motion, vertical mixing, and ocean currents. The climatological ocean currents adjacent to the bottom vary with season and bathymetric depth. They are primarily southward in winter and northward in summer in the south of ~42°N in the GLORYS reanalysis (Figure S7 in Supporting Information S1). We note that mixing and advection influence well-defined scalar fields including the mixed layer and thermocline depth, vertical temperature gradients, and horizontal currents, so here we examine statistical relationships between anomalies in BWT and these variables. The direct impacts of wind-driven and boundary effects are explored in Section 3.4.

The local ACCs between BWT and mixed layer depth (MLD), thermocline depth (TD), thermocline gradient (∇T_{Thrm}), vertical temperature gradient near the bottom (∇T_{Bot}), and currents in the bottom layer in the meridional (V_{Bot}) and zonal (U_{Bot}) direction are shown in Figure 4 for winter and summer. ACC values are presented for locations within 150 km of the coast, where the bathymetric depth is less than 400 m; statistically significant grid squares (t-statistic values exceeding the 95% confidence interval) are color-shaded not-significant values are gray and those where the seasonal thermocline properties are always undefined (see Section 2) are black. BWT-MLD ACC values are large and positive over much of the domain in winter and between 24° and 34°N in summer with ACCs >0.7 over much of the shelf in S and SC in both seasons. Similarly, the BWT-TD ACC values are positive over most of the S and SC regions in both winter and summer with ACCs >0.5 at many grid squares in these regions. Higher ACCs also occur north of ~42°N in summer. Anomaly correlations between BWT and ∇T_{Thrm} are of mixed sign and relatively small amplitude in winter with generally positive values south of 26°N. In contrast, they are negative south of ~34°N with larger magnitude ACC values along the wider portions of the shelf at 26°N and 28°N during summer. ACCs between BWT and ∇T_{Bot} are generally positive especially for offshore locations in JFM and in nearshore regions north of 40°N and at approximately 26°, 28°, and 34°–37°N in JAS. The BWT anomaly correlations with the bottom currents tend to be of opposite sign with positive values for

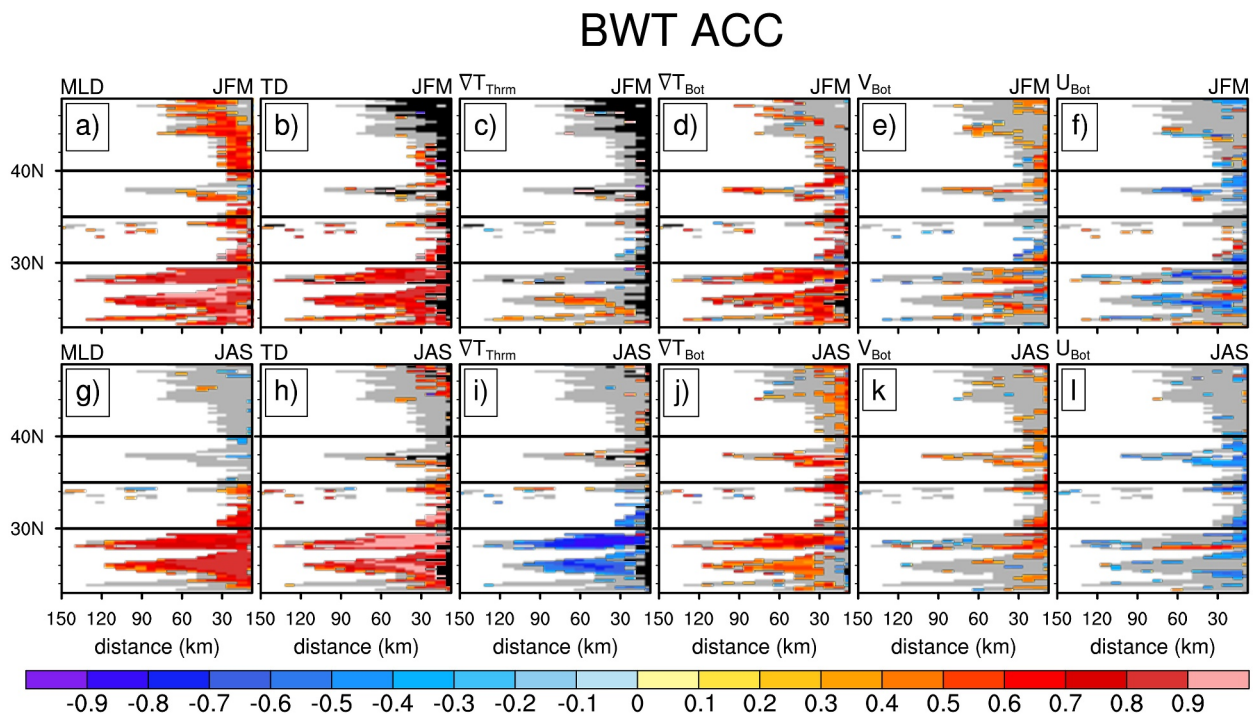

Figure 4. Correlations between BWT anomalies and six ocean variables at each model grid square on the shelf. The seasonal average anomaly correlation coefficient (ACC) for BWT with (a, g) Mixed Layer Depth (MLD), (b, h) thermocline depth (TD), (c, i) thermocline gradient (∇T_{Thrm}), (d, j) vertical bottom temperature gradient (∇T_{Bot}), (e, k) bottom meridional velocity (V_{Bot}), and (f, l) and bottom zonal velocity (U_{Bot}) for (top) JFM and (bottom) JAS. Black lines delineate the four regions defined in Figure 1; black squares indicate where the thermocline is undefined and gray squares where the correlations are not significant based on the t-statistic at the 95% confidence level.

V_{Bot} and negative for U_{Bot} (also see Figures S8 and S9 in Supporting Information S1). The zonal and meridional heat transport in the bottom layer are also anticorrelated, but when combined they are positively correlated with BWT anomalies at a number of grid squares in the N region during JFM but not during JAS (Figure S10 in Supporting Information S1).

Positive correlations for MLD and TD in Figure 4 indicate that BWTs are anomalously warm when the mixed layer and thermocline are deeper consistent with warmer surface waters extending toward the bottom. The negative correlations between ∇T_{Thrm} and BWT in summer may reflect a vertical spreading (weakening) of the thermocline and potentially more warm water reaching the bottom. The positive ∇T_{Bot}–BWT correlations suggest that enhancing the gradient near the bottom will increase temperatures perhaps in conjunction with a deeper thermocline bringing warm water close to the bottom. Positive BWT-V ACC values are consistent with an increase in poleward currents enhancing transport of warmer water along the shelf, while enhanced onshore flow ($U > 0$) at depth would advect colder water along the bottom (also see Figure S9 in Supporting Information S1). U and V may be anticorrelated, since poleward currents would result in westward currents due to mass conservation and deflection by a southeast to northwest oriented coastline.

The predictors used in the correlation analysis are not independent of each other at some locations, as indicated by the regional averages of the local ACC values between MLD, TD, ∇T_{Thrm}, and ∇T_{Bot} in JFM (Figure S8 in Supporting Information S1) and JAS (Figure S9 in Supporting Information S1). Although the correlations vary widely by variable and region, they can be quite high, for example, TD is significantly correlated (or anti-correlated) with the other predictor variables especially in summer. To partly address this issue we use multiple linear regression (MLR), which subtracts collinearity between predictor variables to further discern the relative strength of their individual relationship with BWT anomalies. The regression values between BWT and the six predictor variables, normalized by the local standard deviation, are shown in Figure 5. To obtain a more comprehensive view of the MLR analysis, regionally averaged results, including nearshore (bottom depth <100 m) and offshore (100 m <bottom depth <400 m) areas, are also presented. This includes the fractional

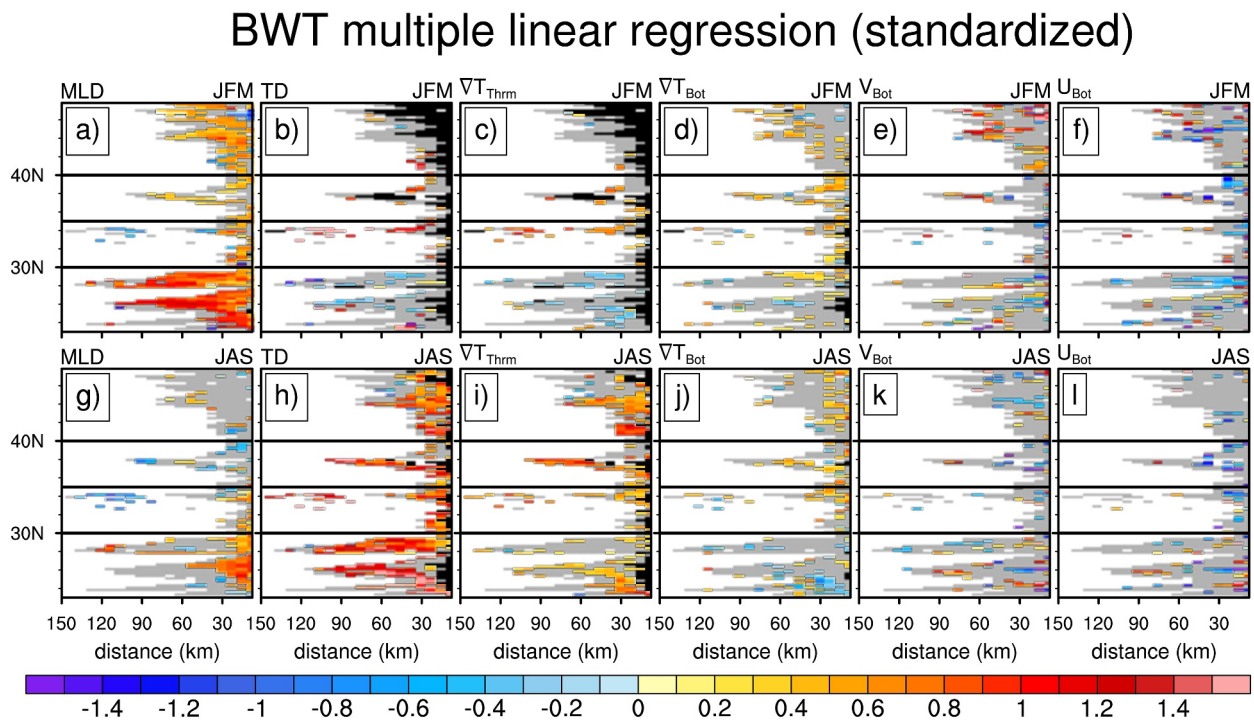

Figure 5. Values from a multilinear regression model from six predictor ocean variables BWT anomalies. Standardized regression coefficients from a Multilinear Regression (MLR) model for the predictors: (a, g) MLD, (b, h) TD, (c, i) ∇T_{Bot}, (d,j) ∇T_{Bot}, (e, k) V_{Bot}, and (f, l) U_{Bot} for (top) JFM and (bottom) JAS. Colored areas indicate significant regression coefficients (90%) and gray areas are not significant. Black squares indicate where the thermocline is undefined; black lines delineate the four regions defined in Figure 1.

area of a region with significant regression values shown in Figure 6 and the average of the regression values in Figure 7.

The efficacy of the BWT predictors varies by season, region, and depth. MLD is the leading predictor of BWT anomalies during winter over much of the domain especially nearshore in the N and S regions. MLD-BWT regression values exceed 0.5 and 1.0 at many grid points in the N and S regions, respectively. In contrast, TD is the dominant predictor during summer, especially offshore, whereas significant MLD regression values only occur nearshore in the S and SC regions. The ∇T_{Thrm} regressions are also positive in summer albeit with fewer significant values and smaller amplitudes than TD. The negative ACC values in S during summer (Figure 4i) are not seen in the regression values, which are either not significant or positive (Figure 5i), suggesting that its correlation with BWT anomalies could be explained by covariability with other predictors. Statistically significant ∇T_{Bot}-BWT regression values are generally positive in the three northern regions but have modest amplitudes and are somewhat scattered across the shelf. Although the overall regression values for the bottom currents are relatively small, V-BWT correlations are positive (i.e., northward current anomalies are associated with warmer BWT) with sizable amplitudes during winter in N. Eastward current anomalies tend to damp BWT anomalies especially in shallow regions during summer in the three northern regions (Figure 7).

Although not the main goal of the MLR analyses, it's still worthwhile to assess its overall skill as a predictor of BWT anomalies. The correlations between the predicted and observed BWT anomalies, using all six predictor variables, indicate the MLR is skillful at nearly all points with values exceeding 0.7 over the majority of grid cells (Figure S11 in Supporting Information S1). The main exception is for offshore points during JAS at ~24°N and north of 40°N. However, the BWT variability is very low in the N region with $\boldsymbol{\sigma}$ values generally less than 0.4°C. We also assessed the MLR using the Akaike information criterion (AIC, Akaike, 1974; Burnham & Anderson, 2002), which imposes a penalty for adding variables to the prediction system in order to reduce the likelihood of overfitting (e.g., Wilks, 2020). Although the optimum model using the AIC criteria varies by location, the best model overall includes all six predictor variables (Figure S12 in Supporting Information S1).

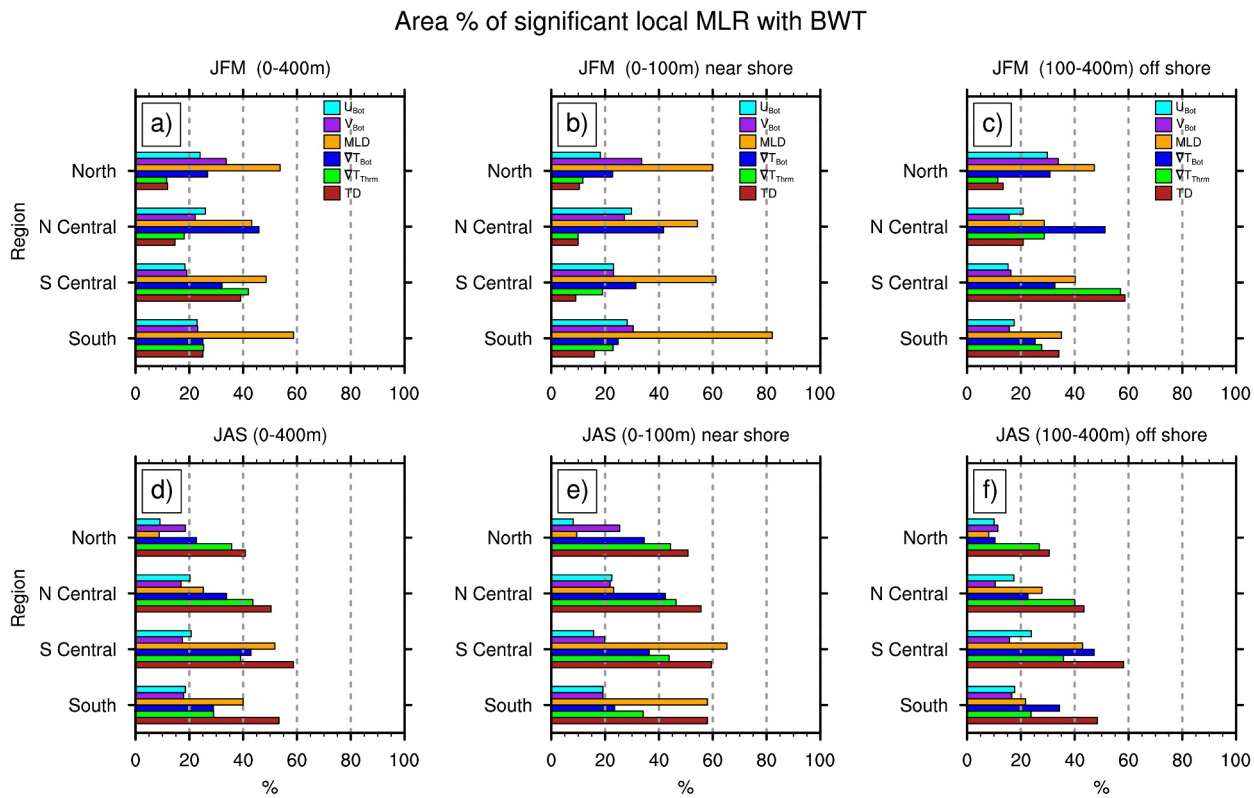

Figure 6. Percentage of the shelf area over the four regions with significant regression coefficients shown in Figure 5 for the (a, d) entire shelf (≤400 m deep), (b, e) near shore (<100 m deep), and (c, f) offshore (100–400 m deep) in (top) JFM and (bottom) JAS.

3.3. Temporal Variability of Boundary Processes

Variability in the CCS is influenced by CTWs, particularly Kelvin waves, that propagate northward along the West Coast of North America. Individual waves, clearly evident in SSH variability, propagate rapidly (~2.7 m s^{-1} for the first baroclinic mode), whereas their cumulative effects associated with ENSO impact the SSH on interannual timescales. Here, we explore how these processes influence bottom temperatures using daily GLORYS data. To identify timescales for the wave-related processes, cross spectra are computed between SSH near Cabo San Lucas ("Cabo") at the southern tip of Baja California (SSH averaged over ~23°N–23.5°N) and SSH northward along the coast (Figure 8, top row). SSH variability is coherent over nearly all timescales south of ~30°N and over much of the domain for periods of approximately 40–180 days and longer than ~9 months. For periods <~3 months, the Cabo SSH lead SSH anomalies further north with those poleward of 40°N lagging the anomalies at Cabo by approximately 20 days (Figures 8b and 8c). At annual and longer timescales, the SSH anomalies are nearly in phase over the domain, although those further north slightly lead (10–20 days) those at Cabo perhaps due to wind forcing or difficulty in distinguishing the phase for longer periods in the relatively short record. Cross spectra analysis between SSH at Cabo and BWT as a function of latitude (Figure 8, bottom row) is generally similar to the SSH analysis, except there is less coherence for timescales shorter than ~9 months and the lags are longer. For periods longer than a year, there is also strong coherence throughout the domain with the BWT anomalies lagging Cabo SSH by 10 to more than 30 days. The Cabo SSH-BWT cross spectra results suggest that the processes influencing SSH on subannual and interannual timescales also influence BWT anomalies.

3.3.1. Intraannual Timescales

Based on the cross spectral results, and following Amaya et al. (2022), we time filtered the SSH data retaining periods of 20–180 days to isolate the variability associated with coastally trapped waves. Correlations of the Cabo SSH anomalies with those further north are shown in Figure 9a. The positive values are both followed and preceded by negative values, suggesting oscillatory behavior with a period of 50–60 days. High correlation values

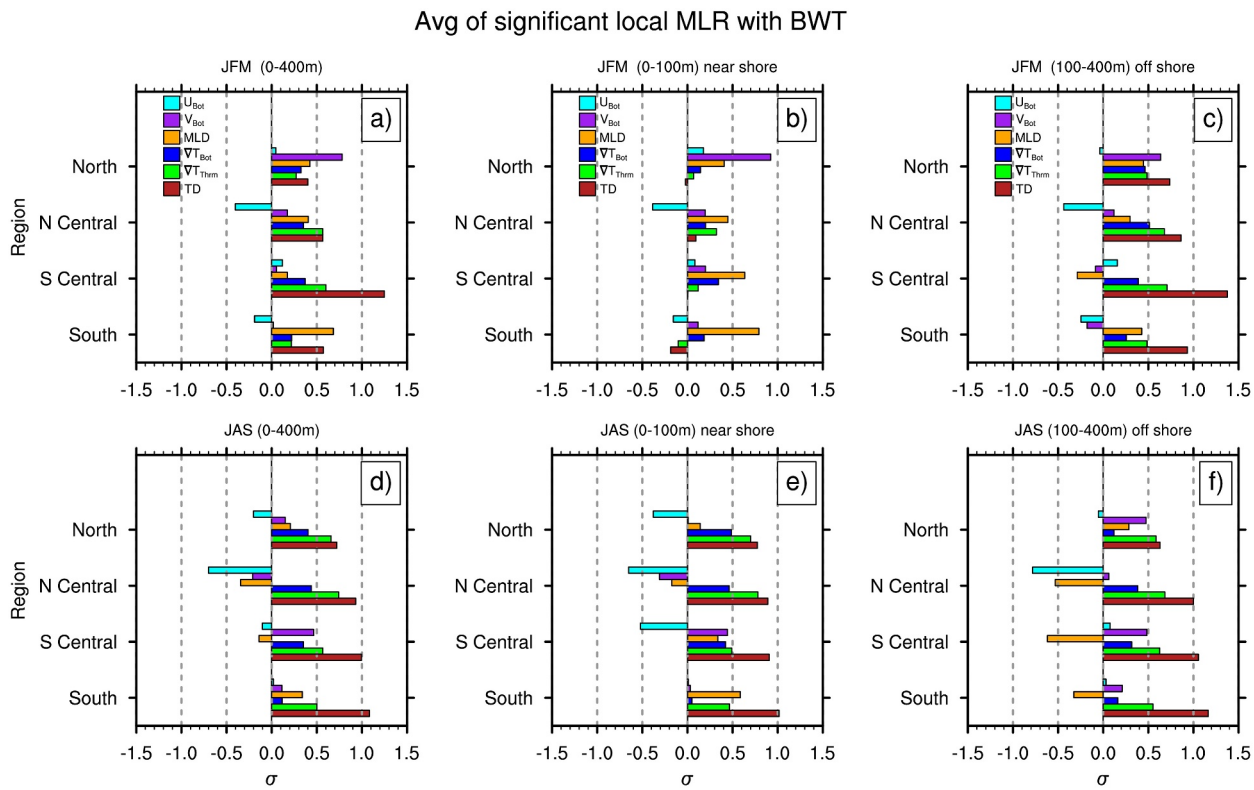

Figure 7. Area average over the four regions of the significant regression coefficients shown in Figure 5 for the (a, d) entire shelf, (b, e) near shore, and (c, f) offshore during (top) JFM and (bottom) JAS.

(ACC >0.6) extend to ~38°N, where they lag those at Cabo by approximately 6 days. The correlations diminish with distance from Cabo with values of ~0.3 at 50°N at a lag of ~10 days. The cross spectra and correlation analyses are consistent with the period and propagation speed of CTWs in previous studies (e.g., Amaya et al., 2022).

Correlations between the time filtered SSH at Cabo and BWT anomalies as a function of latitude (Figure 9b) exhibit a similar structure as those for SSH but with reduced amplitude: ACC >0.3 extend to ~36°N. However, the *local* correlation between the temporally filtered SSH and BWT anomalies (Figure 9c) show ACCs > 0.5 at nearly all latitudes with positive values lasting for ~20 days and generally reaching a maximum when the BWT lags the SSH anomalies by 2–5 days. The results suggest that, while CTWs can influence the bottom temperature as they propagate northward (Figure 9b), other processes, such as wind-driven changes in SSH, also influence BWTs within a few days.

3.3.2. Interannual Timescales: ENSO

The cross spectral analysis indicates a strongly coherent coastal signal in SSH and BWT anomalies at interannual (>~9 months) timescales. Given that basin-scale phenomena, for example, ENSO, PDO, and NPGO operate on these timescales, we correlate BWT anomalies at Cabo averaged over November–January with SSH anomalies over the Pacific Basin (10°S–60°N) at 3-month intervals (Figure 10). Positive correlation values extend across the tropical Pacific with a maximum in the vicinity of the dateline when the basin anomalies lead the Cabo BWT anomalies by 9 months. Positive correlation values occur along the entire West Coast of North America at 6 months lead. As lags decrease, positive values on the equator extend eastward and intensify near the coast of South America. The largest values occur along the entire West Coast in December (0 lag) with ACCs >0.9 off southern Baja and >0.6 along the US West Coast. Negative values extend eastward across the equatorial Pacific over time and cover the entire basin when lagging the Cabo BWT values by 6 months. Positive ACCs still extend along the West Coast of North America at 3 months lag and decrease in amplitude and shift offshore at some latitudes. Correlations between Cabo SSH and Pacific basin SSH (Figure S13 in Supporting Information S1) and

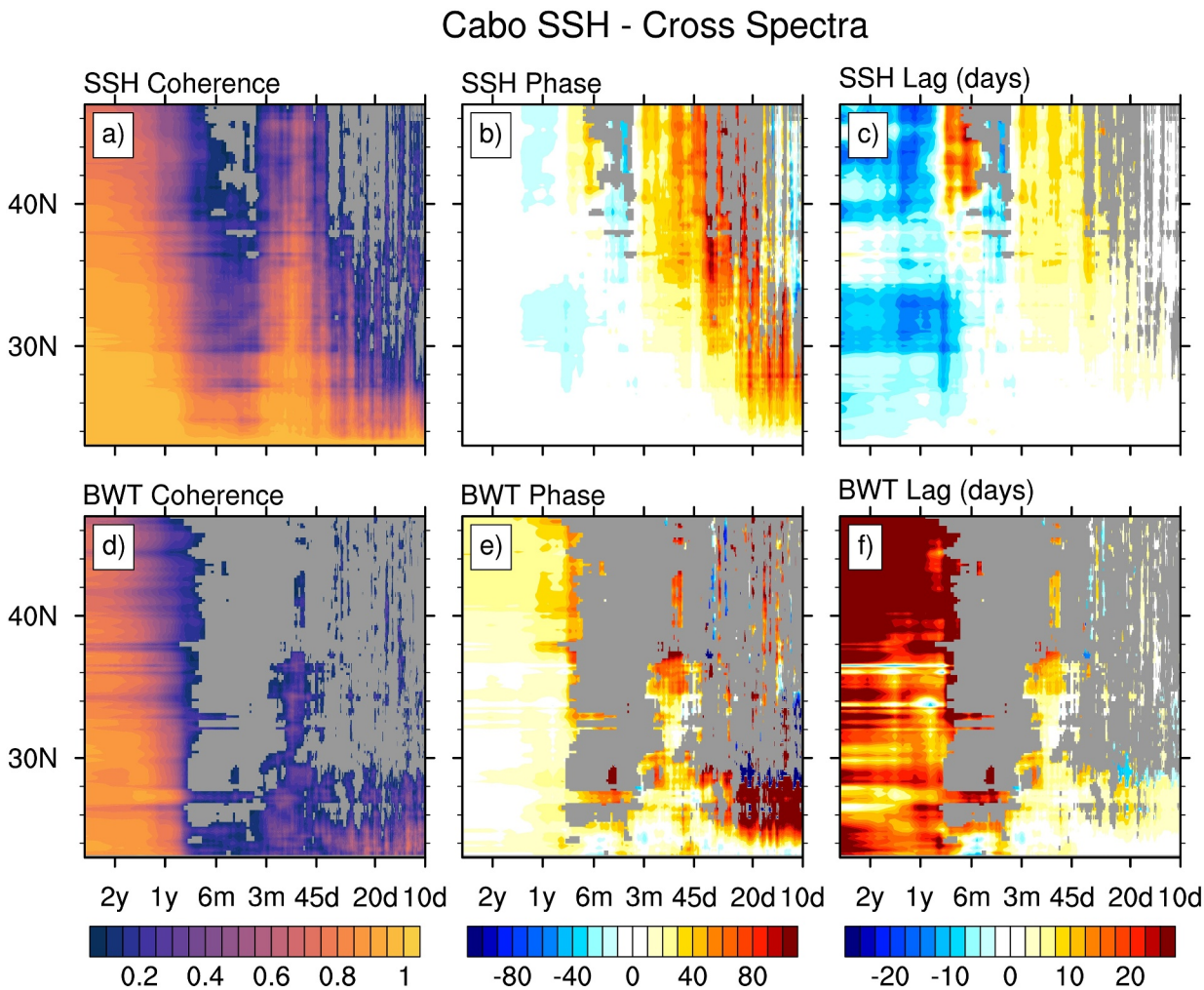

Figure 8. The relationship between SSH at the southern end of the domain and SSH and BWT anomalies within the domain as a function of frequency/period, which is useful for identifying propagating features, including coastally trapped waves (CTWs). Cross spectra showing the (a, d) Coherence, (b, e) phase and (c, f) lag in days between the southern Baja California ("Cabo," 23°N–23.5°N) SSH and coastal (nearest 0.5° longitude to shore) for (a–c) SSH and (d–f) BWT (<400 m) as a function of latitude. A positive phase or lag indicates that the Cabo SSH index leads the SSH and BWT at higher latitudes. Gray indicates points where the coherence is not significant (at the 90% level).

SSTs (Figure S14 in Supporting Information S1) are similar to those in Figure 10. These figures clearly reflect the influence of ENSO on the Pacific basin, including the eastward extension of SSH and SST anomalies along the equator and surface and bottom conditions along the West Coast of North America.

To further investigate the influence of ENSO on BWT along the West Coast, regression values between Nino 3.4 (5°N–5°S, 120°W–170°W) SST anomalies in November-January and monthly BWT anomalies from 23°N to 50°N are shown in Figure 11. Regression values are near zero over the entire West Coast domain in June, 6 months prior (lag −6) to the ENSO index. Progressing through boreal summer, fall, and winter, the values generally increase with values exceeding 1°C/(+1σ Nino3.4) over many grid cells south of 32°N and 0.5°C/(+1σ Nino3.4) north of this latitude. Large values extend across the shelf with maximum values often occurring offshore. For example, regression values >2°C/(Nino3.4°C) at ∼30 km from the coast at 24°N at lags of −1 to +2 months. Although the ENSO related anomalies are nearly concurrent over the domain, the regressed BWT anomalies appear first in the south and exhibit some northward progression with time especially between 24° and 34°N at leads of 5 to 2 months, possibly as a result of the integrated effects of multiple ENSO-driven CTWs. The anomalies decay at lags longer than ∼3 months (not shown).

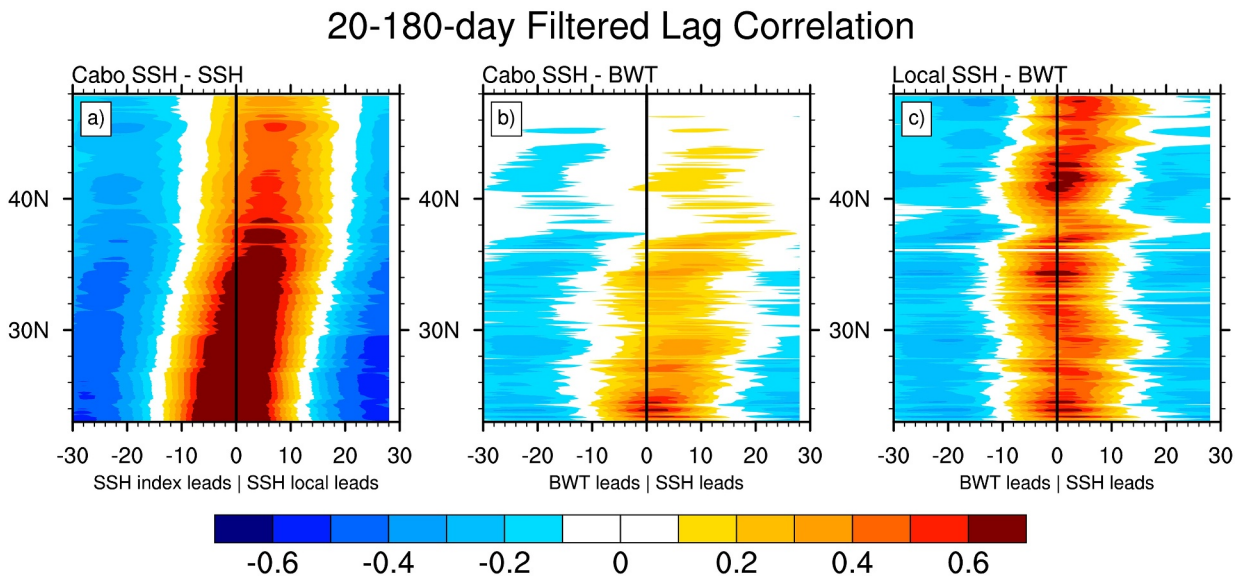

Figure 9. Lead-lag correlations as a function of latitude for time filtered (20–180 days band pass) coastal (nearest 0.5° longitude to shore) averaged anomalies between Cabo SSH anomalies and (a) SSH anomalies and (b) BWT (≤400 m) anomalies and (c) between the collocated SSH and BWT anomalies.

3.4. Surface and Ocean Boundary Forcing: Wind and Waves

Wind-driven Ekman pumping can influence CCS BWT through local variations in the vertical velocity and by exciting propagating phenomena, including CTWs within and/or to the south of our domain, that generate SSH and subsequently temperature and current anomalies at depth that influence BWT. To identify the relative contribution of each of these processes to BWT variability in the CCS, we use a ROMS control simulation (Section 2.2) forced by time varying surface and ocean boundary conditions in addition to GLORYS. Ekman effects associated with surface wind forcing are computed using the Coastal Upwelling Transport Index (CUTI, Jacox et al., 2018), which includes vertical motion driven by the wind stress curl in addition to alongshore wind stress. The influence of CTWs is obtained from SSH anomalies at 30.5–31.0°N near the southern boundary of the ROMS domain. In GLORYS, correlations between the southern boundary SSH and coastal ocean conditions decrease from 30.5 to 48°N with ACCs declining from 0.9 to 0.7, 0.8 to 0.4, and 0.7 to 0.3 for SSH, BWT and SST, respectively (Figure 12; pink) based on 8-day averages. In contrast, there is an increase in ACCs with latitude between CUTI and coastal conditions in GLORYS, although the values are generally small (<0.4) and are less than those associated with the southern boundary SSH throughout the domain. The main exception is for correlations with SST in the northern half of the domain, where they are of comparable magnitude (~0.4). The ROMS ACCs are similar to those from GLORYS, except they are higher for CUTI-SSH near ~40°N and lower in the northern and southern parts of the domain for CUTI-BWT. The results for winter and summer, based on 8-day lags using the Cabo SSH index from GLORYS (Figure S14 in Supporting Information S1), are similar to those in Figure 12 except with stronger declines in ACCs with latitude during summer with the SSH index.

We further examine the role of boundary forcings on BWT anomalies using ROMS sensitivity experiments including a "Wind" simulation in which the full surface wind stress forcing is applied but with seasonally varying climatological values at the ocean boundaries and an "Ocean" simulation where the ocean boundary conditions are variable but the surface forcing is climatological. Comparing variability in the ocean and wind experiments to the control run (with full realistic forcing) allows us to isolate the influences of local winds and remote ocean forcing on bottom temperatures (Figure 13). ACCs between the BWT anomalies in the control and wind simulations increase with latitude from 0.41 to 0.63 to 0.78 in the SC, NC and N regions, whereas ACCs between BWT anomalies in the control and ocean simulations decrease with latitude from 0.89 to 0.74 to 0.61, respectively. Note the southern region is outside the ROMS domain. These results indicate that bottom temperature is more strongly influenced by ocean (wind) forcing in the southern (northern) part of the domain consistent with previous analyses of other ocean variables (e.g., Frischknecht et al., 2015). Furthermore, comparing Figures 12 and 13 indicates that the full influence of the wind stress on BWT anomalies (Figure 13) is greater than just the influence of local wind-

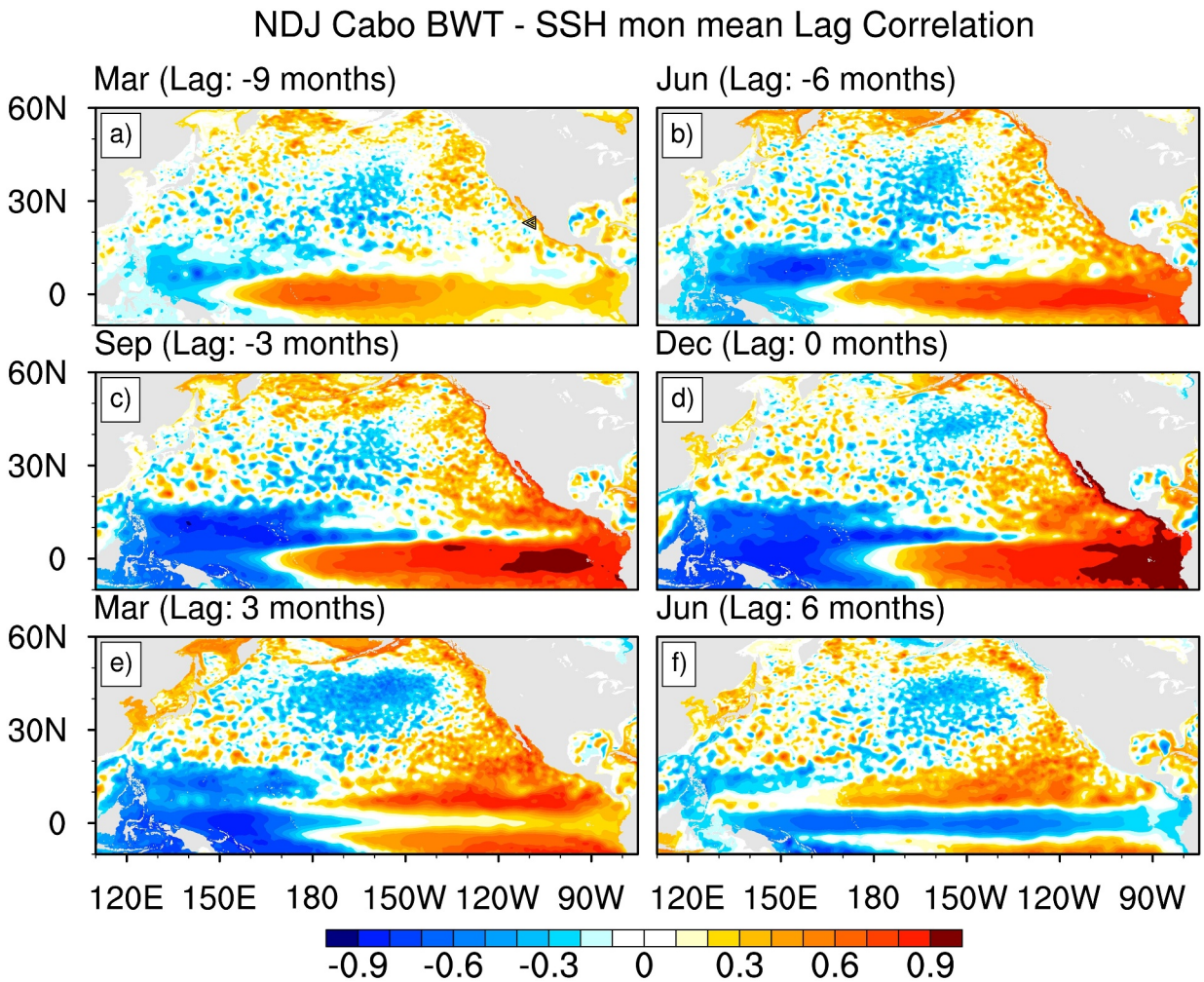

Figure 10. Evolving basin-wide SSH anomaly patterns that are related to BWTs at the southern end of the CCS reveal ENSO's influence. Correlations between the Cabo BWT anomalies averaged across the shelf (23°N–23.5°N, 0.5° longitude nearest the coast, ≤400 m deep) during NDJ with the monthly mean SSH anomalies over the Pacific from 10°S to 60°N at lags of (a) −9, (b) −6, (c) −3, (d) 0, (e) 3, and (f) 6 months, which range from the previous March to the following June. A negative lag indicates the SSH anomalies precede the Cabo BWT index. The location of the Cabo index is depicted by a triangle in panel (a).

driven upwelling (Figure 12). This difference could be due to nonlocal impacts of wind stress, for example, CTWs and eddies that are generated and propagate within the coastal domain. Although surface heat flux forcing is critical for creating SST anomalies in the open ocean (e.g., Alexander et al., 2002), it had a negligible impact on coastal BWT anomalies in a sensitivity experiment with variable surface heat flux forcing and climatological wind stress and ocean boundary conditions (not shown).

4. Discussion and Conclusions

Given the sparse measurements and limited analyses of bottom water temperature, we use GLORYS, a high resolution ocean reanalysis, to examine BWT anomalies and the processes that influence them on the continental shelf (<400 m depth) along the West Coast of North America. BWT variability in the 27-year record (1993–2019) is exceptionally strong in portions of southern Baja ($\sigma > 2$°C) with periods where the anomalies exceed those at the surface and can be associated with intense bottom marine heatwaves (Amaya, Alexander, Jacox, Scott, et al., 2023). BWT exhibits substantial interannual variability (0.5°C < σ < 1°C) over much of the shelf except for offshore locations north of ~40°N in summer (0.5°C < σ). The BWT anomalies are coherent over the domain with slightly stronger correlations between regions than for SST anomalies. Like SST and SSH anomalies, the large and coherent BWT anomalies on interannual timescales are clearly associated with ENSO (also see Amaya, Alexander, Jacox, Scott, et al., 2023; Xu et al., 2024).

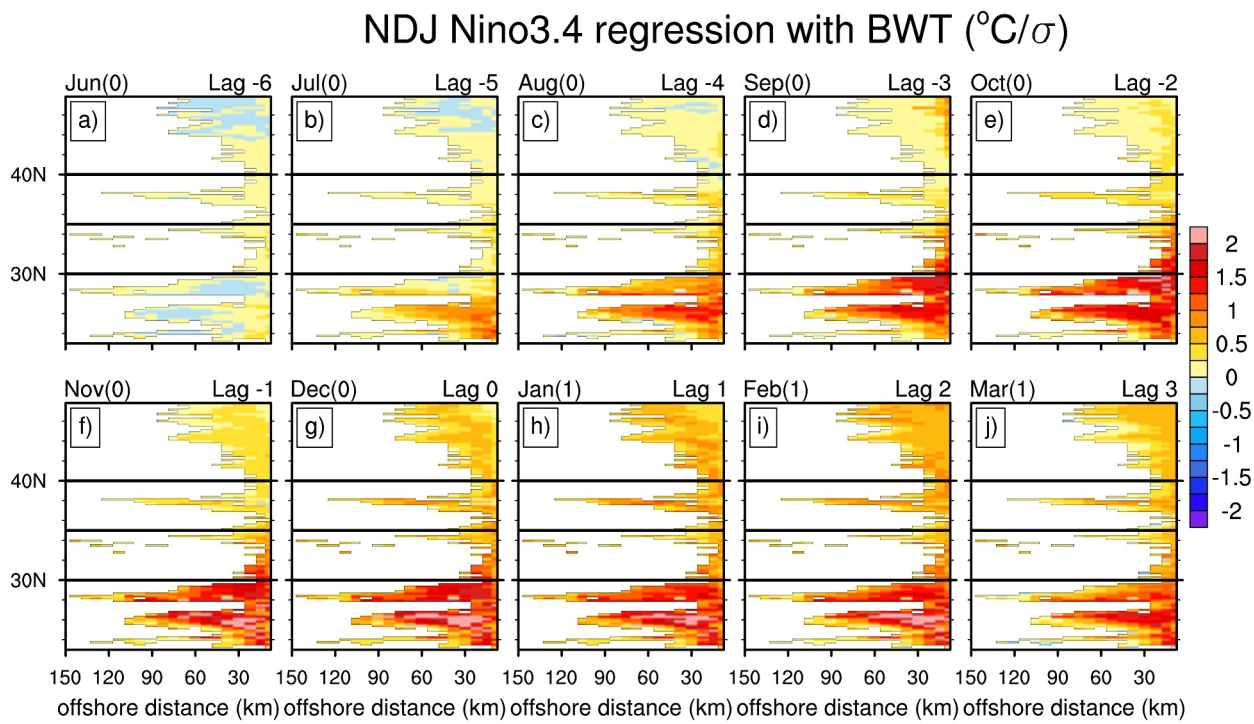

Figure 11. The influence of ENSO on BWT anomalies on the shelf in the CCS. Monthly BWT anomalies on the shelf between 23°N and 50°N regressed on the NDJ Niño 3.4 (5°S–5°N, 170°W–120°W) SST anomalies. Regression values (°C/Nino SST σ) are for shown for (a) June prior to the Nino index (−6 months lag) to the following (j) March (+3 months lag).

We have used correlation and multiple linear regression analyses to examine the linear relationship between collocated BWTs and ocean variables, including the mixed layer depth, thermocline depth and strength, bottom temperature gradient and currents. Although anomalies in all of these variables are related to BWT anomalies in some locations, the dominant factors coastwide were MLD during winter and thermocline depth in summer; MLD is also important nearshore south of 30°N in summer, although this may be an indirect effect as the mixed layer is shallow (<15 m) in this area (Figure S1 in Supporting Information S1). We note that many of the predictor variables in the MLR were not independent from each other in some locations. For example, during the strong El Niño event in 2016, the mixed layer and thermocline deepened and the thermocline and bottom temperature gradient strengthened (Figure 14), which contributes to the positive BWT anomalies west of Baja California.

Although the MLR removes the covariability between predictors, it's difficult to definitively determine which has the greatest effect on BWT anomalies. This suggests that using a high-resolution ocean model simulation driven by observed boundary conditions, with fields archived to compute heat budgets, could be helpful to better understand the processes that influence bottom water conditions on continental shelves. This approach has been used for surface temperature anomalies (Chao et al., 2017). In addition, state estimations, such as Estimating the Circulation and Climate of the Ocean (ECCO, Forget et al., 2015), which are similar to reanalyses but conserve properties by adjusting forcing as well as the ocean variables, are designed for this purpose. To date, however, these global state estimates have been at coarser resolution and with values that are further from observations compared to high-resolution reanalyses (Castillo-Trujillo et al., 2023).

Although the MLR model used here estimates the local concurrent BWT anomalies reasonably well, other predictor variables and more rigorous out-of-sample testing should be explored to reconstruct or predict bottom water temperatures. For example, Kavanaugh et al. (2017) used an MLR that included SSTs, SSH, surface wind stress, and large-scale climate indices as predictors, although high-resolution ocean reanalyses may alleviate the need to use statistical methods to estimate BWT. Empirical methods, however, may still be quite useful for predicting future BWT anomalies. Using a linear inverse model with SST and SSH over Pacific Basin and BWTs from GLORYS as input, Xu et al. (2024) skillfully predicted BWTs along the West Coast of North America on

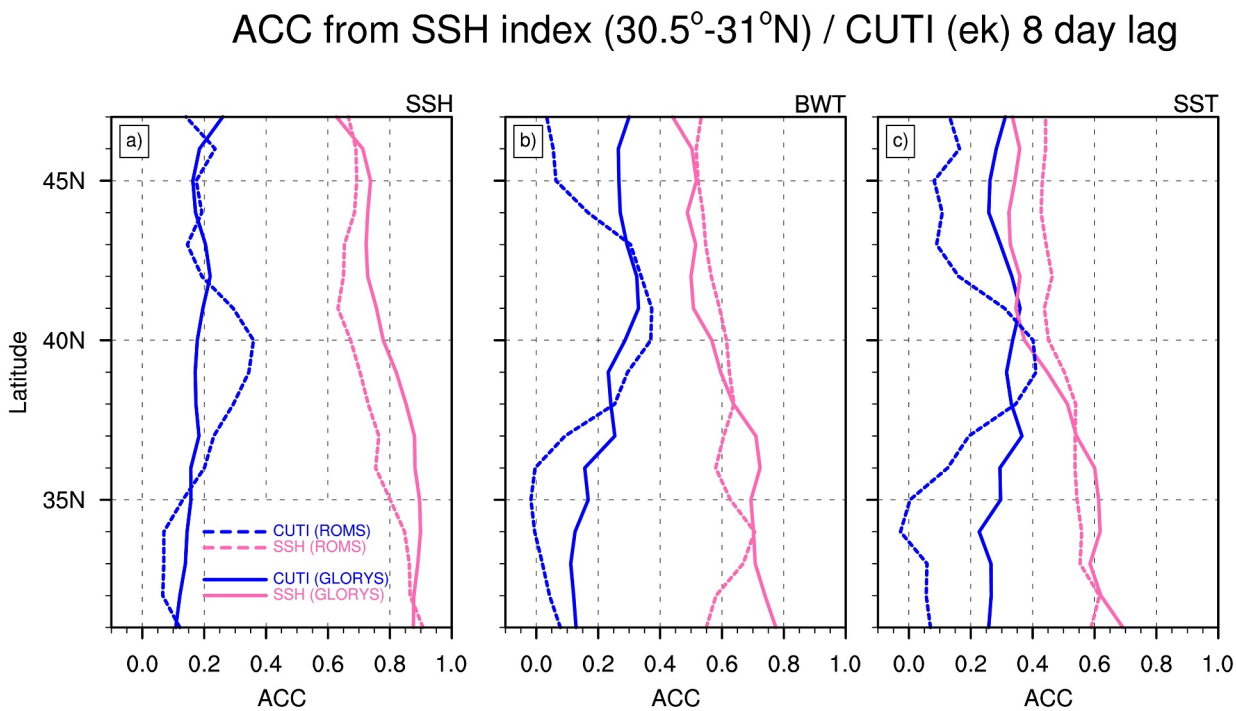

Figure 12. The influence of local winds and poleward propagating CTWs on SSH, BWT, and SST anomalies in the CCS. ACCs as a function of latitude averaged over the continental shelf (<400 m) for (a) SSH, (b) BWT, (c) SST with the SSH anomalies at 30.5°N–31°N (pink), and the local wind-driven component of the Coastal Upwelling Transport Index (−1*CUTI, blue) for GLORYS (solid) and ROMS (dashed). The ACC values are computed daily based on 8-day averages (the archived frequency of the ROMS output), where the anomalies lag the SSH and CUTI indices by one 8-day period. Given the large number of samples, results in low ACC values (<0.1) being statistically significant based on two sided *t*-test at a 95% confidence level even after taking the autocorrelation in the variables into account. The wind-driven component of CUTI is driven by alongshore winds and wind stress curl (Jacox et al., 2018).

seasonal timescales, while Chen et al. (2021) developed an empirical system for predicting BWT anomalies on the northeast US shelf.

The BWT and overlying SST anomalies are well correlated over most of the domain particularly in winter; the main exception occurs offshore north of ∼42°N (Figure 2). As indicated by the MLR analysis and previous studies (Alexander et al., 2023; Amaya, Alexander, Jacox, Scott, et al., 2023; Richaud et al., 2016), the MLD can be a key link between SST and BWT, when it extends to the bottom the two are directly connected. In the northeast Pacific, the mean MLDs are shallow generally less than 60 m on the shelf in winter and 20 m in summer (Figure S1 in Supporting Information S1), which contributes to the stronger influence of MLD variability on BWT anomalies in winter, whereas the rapid dropoff of the continental shelf confines its influence to nearshore regions in summer. Since the temperature decreases with depth along the West Coast, mixing surface waters deeper will result in warmer temperatures near the bottom, resulting in positive SST-BWT and MLD-BWT correlations. Although turbulence generated by wind stirring and surface buoyancy forcing influence MLD, it is likely that dynamical ocean processes play a critical role in setting the MLD along the West Coast of North America. The very strong vertical density gradient near the top of the thermocline restricts the depth to which the mixed layer penetrates. Wind and eddy driven upwelling, ocean eddies, and CTWs vertically displace the pycnocline, thereby influencing the mixed layer as well as the thermocline depth. Upwelling and the strength of the thermocline are especially strong in summer.

As in previous studies, our analyses of SSH anomalies show clear evidence of poleward propagation along the West Coast of North America, likely associated with Kelvin and other CTWs. The waves, with preferred periods between roughly 30 and 90 days, propagate rapidly, moving along the coast from the southern tip of Baja California (∼23°N) to the Canadian border (∼50°N) in approximately 10–20 days. The coastal BWT anomalies track the overlying SSH anomalies with a maximum correlation at a lag of 2–5 days. Thus, BWT anomalies also propagate northward on these subseasonal timescales, although their amplitude substantially decreases with latitude. On interannual timescales, the anomalies in SSH, BWT, and SST are nearly in phase and coherent along

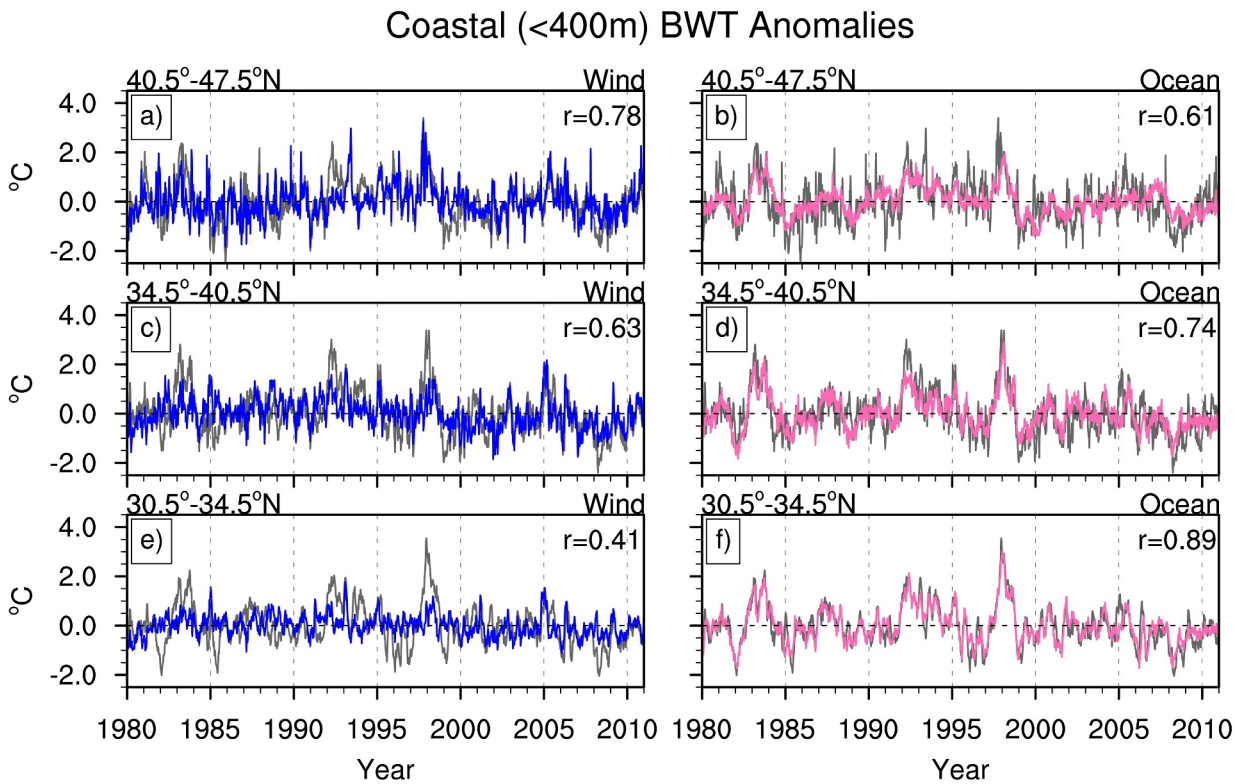

Figure 13. The influence of wind forcing and ocean boundary conditions, including CTWs, on BWTs in the CCS obtained using model sensitivity studies. Time series of BWT anomalies on the shelf (<400 m) averaged the north, north central, and south central regions. The control with full forcing and variable wind and ocean sensitivity simulations (in which the other forcing fields are set to their respective climatology) are shown by gray, blue, and pink lines, respectively. The correlation between the control and the sensitivity run is shown in the upper right corner of each panel.

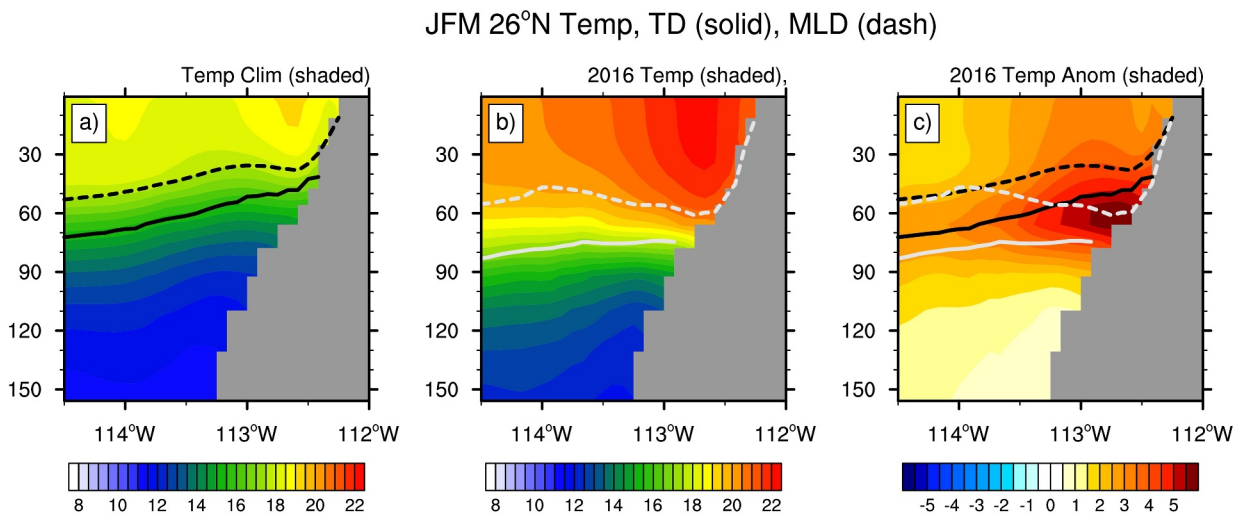

Figure 14. The climatology and changes in the ocean temperature as a function of depth west of Baja California illustrating the large changes in MLD, TD, and vrtival temperature gradients during a strong El Niño event. Cross sections at 26°N during JFM of the temperature (°C, shading), MLD (dashed line), and TD (solid line) for (a) climatology and (b) 2016. (c) Temperature anomalies during JFM 2016 (°C, shading) and the MLD (dashed) and TD (solid) for the climatology (black) and during 2016 (gray).

the entire West Coast of North America in response to ENSO; the relatively short record precluded investigating the influence of decadal variability.

In addition to Kelvin waves that are generated along the equator in the Pacific and then propagate poleward upon reaching the West Coast of the Americas, wind stress variability also influences coastal conditions. Wind-driven upwelling influences local ocean conditions but can also generate coastal trapped waves and eddies. Although the local wind forcing influences SSH, SST, and BWT in the GLORYS reanalysis, its impact is generally smaller than that associated with SSH anomalies at the southern boundary. A regional ocean model simulation with variable surface and boundary conditions produces coastal SSH, SST, and BWT anomalies that are similar to those in GLORYS (Figure 12). Compared to this control simulation, a sensitivity experiment in which the wind stress forcing was set to climatological values but the ocean boundary was variable, confirmed the importance of ocean variability, including poleward propagating CTWs. However, the correlations between BWT anomalies in these two simulations decrease by ~⅓ between the southern and northern part of the domain along the US West Coast (Figure 13), indicating the diminishing impact of CTWs on bottom temperature with an increase in latitude. A complementary experiment with variable wind stress forcing but climatological ocean boundary conditions confirmed that the influence of the wind on BWT anomalies increases with latitude. Comparing this experiment with the control highlighted the importance of nonlocal wind stress forcing within the domain on BWT anomalies. As a result, the full wind forcing has a larger (comparable) impact on BWT anomalies relative to the ocean boundary driven BWT variability off the Pacific Northwest (Central California) coast. An additional sensitivity experiment indicated that surface heat flux anomalies had a negligible impact on BWT anomalies on the shelf adjacent to the US West Coast unlike SST anomalies in the open ocean.

Bottom water temperature strongly influences marine organisms, especially demersal species, and BWTs along the West Coast of North America are both highly variable and warming (Alexander et al., 2023). Given the relatively narrow shelf and importance of mesoscale dynamics in the area, regional ocean predictions (Jacox et al., 2023; Siedlecki et al., 2016; Xu et al., 2024) and projections (Howard et al., 2020; Pozo Buil et al., 2021) have been developed with the aim of supporting decision making related to marine resources. On seasonal timescales, both regional ocean models and empirical models have shown that bottom temperature anomalies along the US West Coast are predictable months in advance (Jacox et al., 2023; Xu et al., 2024); on longer timescales, models show an expected continued warming of bottom temperatures (Liu et al., 2023). A better understanding of the processes that influence BWTs can lead to improvements in models' representation of coastal conditions; for example, upper ocean stratification is more predictable than MLD (Jacox et al., 2023), so BWT changes associated with the former may also be more predictable. Better representation of the relevant drivers of BWT could lead to improved ocean model forecasts and projections and ultimately aid their use in marine resource applications.

Data Availability Statement

The GLORYS12v1 reanalysis data (Lellouche et al., 2021) are freely available at https://data.marine.copernicus.eu/product/GLOBAL_MULTIYEAR_PHY_001_030/services. The processed data and the NCAR command language (NCL; Version 6.6.2, 2024; https://www.ncl.ucar.edu/) codes used to generate the figures are available at https://scholar.colorado.edu/concern/datasets/db78td953.

Acknowledgments
We thank Nate Mantua for his thoughtful manuscript review and Dmitry Dukhovskoy and Natalie Freeman for their helpful comments on the analyses and a prelimianry version of the manuscript. This research was supported in part by the NOAA cooperative agreement NA22OAR4320151.

References

Akaike, H. (1974). A new look at the statistical model identification. *IEEE Transactions on Automatic Control*, *19*(6), 716–723. https://doi.org/10.1109/tac.1974.1100705

Alexander, M. A., Bladé, I., Newman, M., Lanzante, J. R., Lau, N., & Scott, J. D. (2002). The Atmospheric bridge: The influence of ENSO teleconnections on air–sea interaction over the global oceans. *Journal of Climate*, *15*(16), 2205–2231. https://doi.org/10.1175/1520-0442(2002)015<2205:TABTIO>2.0.CO;2

Alexander, M. A., Scott, J. D., Friedland, K. D., Mills, K. E., Nye, J. A., Pershing, A. J., & Thomas, A. C. (2018). Projected sea surface temperatures over the 21st century: Changes in the mean, variability and extremes for large marine ecosystem regions of Northern Oceans. *Elementa: Science of the Anthropocene*, *6*(1), 9. https://doi.org/10.1525/elementa.191

Alexander, M. A., Scott, J. D., Jacox, M. G., Deser, C., Amaya, D. J., Capotondi, A., & Phillips, A. S. (2023). A survey of coastal conditions around the continental US using a high-resolution ocean reanalysis. *Progress in Oceanography*, *216*, 103055. https://doi.org/10.1016/j.pocean.2023.103055

Amaya, D. J., Alexander, M. A., Jacox, M. G., & Scott, J. D. (2023). An evaluation of high-resolution ocean reanalyses in the California Current System. *Progress in Oceanography*, *210*, 102951. https://doi.org/10.1016/j.pocean.2022.102951

Amaya, D. J., Alexander, M. A., Jacox, M. G., Scott, J. D., Deser, C., Capotondi, A., & Phillips, A. (2023). Bottom marine heatwaves along the continental shelves of North America. *Nature Communications*, *14*(1), 1038. https://doi.org/10.1038/s41467-023-36567-0

Amaya, D. J., Jacox, M. G., Dias, J., Alexander, M. A., Karnauskas, K. B., Scott, J. D., & Gehne, M. (2022). Subseasonal-to-seasonal forecast skill in the California Current System and its connection to coastal Kelvin waves. *Journal of Geophysical Research: Oceans*, *127*(1), e2021JC01789. https://doi.org/10.1029/2021JC017892

Atlas, R., Hoffman, R. N., Ardizzone, J., Leidner, S. M., Jusem, J. C., Smith, D. K., & Gombos, D. (2011). A cross-calibrated, multiplatform ocean surface wind velocity product for meteorological and oceanographic applications. *Bulletin of the American Meteorological Society*, *92*(2), 157–174. https://doi.org/10.1175/2010BAMS2946.1

Barth, J. A., Pierce, S. D., & Smith, R. L. (2000). A separating coastal upwelling jet at Cape Blanco, Oregon and its connection to the California Current System. *Deep Sea Research Part II: Topical Studies in Oceanography*, *47*(5–6), 783–810. ISSN 0967-0645. https://doi.org/10.1016/S0967-0645(99)00127-7

Bindoff, N. L., & Mcdougall, T. J. (1994). Diagnosing climate change and ocean ventilation using hydrographic data. *Journal of Physical Oceanography*, *24*(6), 1137–1152. https://doi.org/10.1175/1520-0485(1994)024<1137:DCCAOV>2.0.CO;2

Bond, N. A., Cronin, M. F., Freeland, H., & Mantua, N. (2015). Causes and impacts of the 2014 warm anomaly in the NE Pacific. *Geophysical Research Letters*, *42*(9), 3414–3420. https://doi.org/10.1002/2015GL063306

Buckley, M. W., DelSole, T., Lozier, M. S., & Li, L. (2019). Predictability of North Atlantic Sea surface temperature and upper-ocean heat content. *Journal of Climate*, *32*(10), 3005–3023. https://doi.org/10.1175/JCLI-D-18-0509.1

Burnham, K. P., & Anderson, D. R. (2002). *Model selection and multimodel inference: A practical information-theoretic approach* (2nd ed.). Springer-Verlag. https://doi.org/10.1007/b97636

Cai, C., Young-Oh Kwon, Y.-O., Chen, Z., & Fratantoni, P. (2021). Mixed layer depth climatology over the northeast U.S. continental shelf (1993–2018). *Continental Shelf Research*, *231*, 104611. ISSN 0278-4343. https://doi.org/10.1016/j.csr.2021.104611

Carton, J. A., & Giese, B. S. (2008). A reanalysis of ocean climate using Simple Ocean Data Assimilation (SODA). *Monthly Weather Review*, *136*(8), 2999–3017. https://doi.org/10.1175/2007MWR1978.1

Castillo-Trujillo, A. C., Kwon, Y.-O., Fratantoni, P., Chen, K., Seo, H., Alexander, M. A., & Saba, V. S. (2023). An evaluation of eight global ocean reanalyses for the Northeast U.S. Continental shelf. *Progress in Oceanography*, *219*, 103126. ISSN 0079-6611. https://doi.org/10.1016/j.pocean.2023.103126

Chao, Y., Farrara, J. D., Bjorkstedt, E., Chai, F., Chavez, F., Rudnik, D. L., et al. (2017). The origins of the anomalous warming in the California coastal ocean and San Francisco Bay during 2014–2016. *Journal of Geophysical Research: Oceans*, *122*(9), 7537–7557. https://doi.org/10.1002/2017JC013120

Checkley, D. M., & Barth, J. A. (2009). Patterns and processes in the California Current System. *Progress in Oceanography*, *83*(1–4), 49–64. https://doi.org/10.1016/j.pocean.2009.07.028

Chen, Z., Kwon, Y.-O., Chen, K., Fratantoni, P., Gawarkiewicz, G., Joyce, T. M., et al. (2021). Seasonal prediction of bottom temperature on the northeast U.S. continental shelf. *Journal of Geophysical Research: Oceans*, *126*(5), e2021JC017187. https://doi.org/10.1029/2021JC017187

Chhak, K., & Di Lorenzo, E. (2007). Decadal variations in the California Current upwelling cells. *Geophysical Research Letters*, *34*(14), L14604. https://doi.org/10.1029/2007GL030203

Clarke, A. J. (1977). Observational and numerical evidence for wind-forced coastal trapped long waves. *Journal of Geophysical Research*, *7*(2), 231–247. https://doi.org/10.1175/1520-0485(1977)007<0231:OANEFW>2.0.CO;2

de Boyer Montégut, C., Madec, G., Fischer, A. S., Lazar, A., & Iudicone, D. (2004). Mixed layer depth over the global ocean: An examination of profile data and a profile-based climatology. *Journal of Geophysical Research*, *109*(C12), C12003. https://doi.org/10.1029/2004JC002378

Dee, D. P., Uppala, S. M., Simmons, A. J., Berrisford, P., Poli, P., Kobayashi, S., et al. (2011). The ERA-Interim reanalysis: Configuration and performance of the data assimilation system. *Quarerly Journal of the Royal Meteorolical Society*, *137*(656), 553–597. https://doi.org/10.1002/qj.828

Di Lorenzo, E., & Mantua, N. (2016). Multi-year persistence of the 2014/15 North Pacific marine heatwave. *Nature Climate Change*, *6*(11), 1042–1047. https://doi.org/10.1038/nclimate3082

Di Lorenzo, E., Schneider, N., Cobb, K. M., Franks, P. J. S., Chhak, K., Miller, A. J., et al. (2008). North Pacific Gyre Oscillation links ocean climate and ecosystem change. *Geophysical Research Letters*, *35*(8), L08607. https://doi.org/10.1029/2007GL032838

Dorman, C. E., & Winant, C. D. (1995). Buoy observations of the atmosphere along the west coast of the United States, 1981–1990. *Journal of Geophysical Research*, *100*(C8), 16029–16044. https://doi.org/10.1029/95JC00964

Enfield, D. B., & Allen, J. S. (1980). On the structure and dynamics of monthly mean sea level anomalies along the Pacific coast of north and South America. *Journal of Physical Oceanography*, *10*(4), 557–578. https://doi.org/10.1175/1520-0485(1980)010<0557:OTSADO>2.0.CO;2

Enfield, D. B., & Allen, J. S. (1983). The generation and propagation of sea level variability along the Pacific coast of Mexico. *Journal of Physical Oceanography*, *13*(6), 1012–1033. https://doi.org/10.1175/1520-0485(1983)013<1012:TGAPOS>2.0.CO;2

Fiedler, P. C. (2010). Comparison of objective descriptions of the thermocline. *Limnology and Oceanography: Methods*, *8*(6), 313–325. https://doi.org/10.4319/lom.2010.8.313

Fiedler, P. C., & Mantua, N. J. (2017). How are warm and cool years in the California Current related to ENSO? *Journal of Geophysical Research: Oceans*, *122*(7), 5936–5951. https://doi.org/10.1002/2017JC013094

Forget, G., Campin, J. M., Heimbach, P., Hill, C. N., Ponte, R. M., & Wunsch, C. (2015). ECCO version 4: An integrated framework for non-linear inverse modeling and global ocean state estimation. *Geoscientific Model Development*, *8*(10), 3071–3104. https://doi.org/10.5194/gmd-8-3071-2015

Frischknecht, M., Münnich, M., & Gruber, N. (2015). Remote versus local influence of ENSO on the California Current System. *Journal of Geophysical Research: Oceans*, *120*(2), 1353–1374. https://doi.org/10.1002/2014JC010531

Gentemann, C. L., Fewings, M. R., & García-Reyes, M. (2017). Satellite sea surface temperatures along the West Coast of the United States during the 2014–2016 northeast Pacific marine heat wave. *Geophysical Research Letters*, *44*(1), 312–319. https://doi.org/10.1002/2016GL071039

Gómez-Valdivia, F., Parés-Sierra, A., & Flores-Morales, A. L. (2017). Semiannual variability of the California undercurrent along the southern California Current System: A tropical generated phenomenon. *Journal of Geophysical Research: Oceans*, *122*, 1574–1589. https://doi.org/10.1002/2016JC012350

Harvey, C. J. (2009). Effects of temperature change on demersal fishes in the California Current: A bioenergetics approach. *Canadian Journal of Fisheries and Aquatic Sciences*, *66*(9), 1449–1461. https://doi.org/10.1139/F09-087

Hermann, A. J., Curchitser, E. N., Haidvogel, D. B., & Dobbins, E. L. (2009). A comparison of remote vs. local influence of El Niño on the coastal circulation of the northeast Pacific. *Deep Sea Research Part II: Topical Studies in Oceanography*, *56*(24), 2427–2443. https://doi.org/10.1016/j.dsr2.2009.02.005

Hickey, B. M. (1979). The California Current System—Hypotheses and facts. *Progress in Oceanography*, *8*(4), 191–279. ISSN 0079-6611. https://doi.org/10.1016/0079-6611(79)90002-8

Hickey, B. M. (1998). Coastal oceanography of western North America from the tip of Baja California to Vancouver Island. In K. H. Brink & A. R. Robinson (Eds.), *The Sea* (Vol. 11, pp. 345–393). Wiley and Sons, Inc.

Howard, E. M., Frenzel, H., Kessouri, F., Renault, L., Bianchi, D., McWilliams, J. C., & Deutsch, C. (2020). Attributing causes of future climate change in the California Current System with multimodel downscaling. *Global Biogeochemical Cycles*, *34*(11), e2020GB006646. https://doi.org/10.1029/2020gb006646

Hughes, C. W., Fukumori, I., Griffies, S. M., Huthnance, J. M., Minobe, S., Spence, P., et al. (2019). Sea level and the role of coastal trapped waves in mediating the influence of the open ocean on the coast. *Surveys in Geophysics*, *40*(6), 1467–1492. https://doi.org/10.1007/s10712-019-09535-x

Jacox, M. G., Alexander, M. A., Stock, C. A., & Hervieux, G. (2019). On the skill of seasonal sea surface temperature forecasts in the California Current System and its connection to ENSO variability. *Climate Dynamics*, *53*(12), 7519–7533. https://doi.org/10.1007/s00382-017-3608-y

Jacox, M. G., Bograd, S. J., Hazen, E. L., & Fiechter, J. (2015). Sensitivity of the California Current nutrient supply to wind, heat, and remote ocean forcing. *Geophysical Research Letters*, *42*(14), 5950–5957. https://doi.org/10.1002/2015GL065147

Jacox, M. G., Edwards, C. A., Hazen, E. L., & Bograd, S. J. (2018). Coastal upwelling revisited: Ekman, Bakun, and improved upwelling indices for the U.S. West Coast. *Journal of Geophysical Research: Oceans*, *123*(10), 7332–7350. https://doi.org/10.1029/2018JC014187

Jacox, M. G., Pozo Buil, M., Brodie, S., Alexander, M. A., Amaya, D. J., Bograd, S. J., et al. (2023). Downscaled seasonal forecasts for the California Current System: Skill assessment and prospects for living marine resource applications. *PLOS Climate*, *2*(10), e0000245. https://doi.org/10.1371/journal.pclm.0000245

Jacox, M. G., Tommasi, D., Alexander, M. A., Hervieux, G., & Stock, C. (2019). Predicting the evolution of the 2014-16 California Current System marine heatwave from an ensemble of coupled global climate forecasts. *Frontiers in Marine Science*, *6*, 497. https://doi.org/10.3389/fmars.2019.00497

Kavanaugh, M. T., Rheuban, J. E., Luis, K. M. A., & Doney, S. C. (2017). Thirty-three years of ocean benthic warming along the U.S. Northeast Continental Shelf and Slope: Patterns, drivers, and ecological consequences. *Journal of Geophysical Research: Oceans*, *122*(12), 9399–9414. https://doi.org/10.1002/2017JC012953

Keller, A. A., Ciannelli, L., Wakefield, W. W., Simon, V., Barth, J. A., & Pierce, S. D. (2015). Occurrence of demersal fishes in relation to near-bottom oxygen levels within the California Current large marine ecosystem. *Fisheries Oceanography*, *24*(2), 162–176. https://doi.org/10.1111/fog.12100

Koehlinger, J. A., Newton, J., Mickett, J., Thompson, L., & Klinger, T. (2023). Large and transient positive temperature anomalies in Washington's coastal nearshore waters during the 2013–2015 northeast Pacific marine heatwave. *PLoS One*, *18*(2), e0280646. https://doi.org/10.1371/journal.pone.0280646

Kurczyn, J. A., Pérez-Brunius, P., López, M., Candela, J., Delgadillo-Hinojosa, F., & García-Mendoza, E. (2019). Water masses and ocean currents over the continental slope off northern Baja California. *Journal of Geophysical Research: Oceans*, *124*(4), 2803–2823. https://doi.org/10.1029/2018JC013962

Lellouche, J. M., Eric, L., Romain, L. G., Gilles, B. B., Angelique, M., Marie, D., et al. (2021). The copernicus global 1/12° oceanic and sea Ice GLORYS12 reanalysis. *Frontiers in Earth Science*, *9*. https://doi.org/10.3389/feart.2021.698876

Liu, O. R., Ward, E. J., Anderson, S. C., Andrews, K. S., Barnett, L. A., Brodie, S., et al. (2023). Species redistribution creates unequal outcomes for multispecies fisheries under projected climate change. *Science Advances*, *9*(33), eadg5468. https://doi.org/10.1126/sciadv.adg5468

Liu, Z., & Alexander, M. A. (2007). Atmospheric bridge, oceanic tunnel and global climatic teleconnections. *Reviews of Geophysics*, *45*(2), RG2005. https://doi.org/10.1029/2005RG000172

Lynn, R. J., & Bograd, S. J. (2002). Dynamic evolution of the 1997–1999 El Niño–La Niña cycle in the southern California Current System. *Progress in Oceanography*, *54*(1–4), 59–75. ISSN 0079-6611. https://doi.org/10.1016/S0079-6611(02)00043-5

Lynn, R. J., Schwing, F. B., & Hayward, T. L. (1995). The effect of the 1991-1993 ENSO on the California Current System. *California Cooperative Oceanic Fisheries Investigations Reports*, 57–71.

Madec, G., & The NEMO Team. (2008). *NEMO ocean engine, Note du Pôle de modélisation* (pp. 1288–1619). Institut Pierre-Simon Laplace (IPSL).

Mantua, N. J., Hare, S. R., Zhang, Y., Wallace, J. M., & Francis, R. C. (1997). A Pacific interdecadal climate oscillation with impacts on salmon production. *Bulletin of the American Meteorological Society*, *78*(6), 1069–1080. https://doi.org/10.1175/1520-0477(1997)078<1069:APICOW>2.0.CO;2

Marchesiello, P., McWilliams, J. C., & Shchepetkin, A. (2003). Equilibrium structure and dynamics of the California Current System. *Journal of Physical Oceanography*, *33*(4), 753–783. https://doi.org/10.1175/1520-0485(2003)33<753:ESADOT>2.0.CO;2

Monterey, G., & Levitus, S. (1997). Seasonal variability of mixed layer depth for the world ocean. In *NOAA atlas NESDIS* (Vol. 14, p. 100). National Oceanic and Atmospheric Administration, Silver Spring.

Morley, J. W., Selden, R. L., Latour, R. J., Frölicher, T. L., Seagraves, R. J., & Pinsky, M. L. (2018). Projecting shifts in thermal habitat for 686 species on the North American continental shelf. *PLoS One*, *13*(5), e0196127. https://doi.org/10.1371/journal.pone.0196127

NCAR Command Language. (2024). NCAR command language (version 6.6.2) [Software]. *NCAR/CISL/VETS*. https://doi.org/10.5065/D6WD3XH5

Pares-Sierra, A., & O'Brien, J. J. (1989). The seasonal and interannual variability of the California Current System: A numerical model. *Journal of Geophysical Research*, *94*(C3), 3159–3180. https://doi.org/10.1029/JC094iC03p03159

Peterson, W. T., Fisher, J. L., Strub, P. T., Du, X., Risien, C., Peterson, J., & Shaw, C. T. (2017). The pelagic ecosystem in the Northern California Current off Oregon during the 2014–2016 warm anomalies within the context of the past 20 years. *Journal of Geophysical Research: Oceans*, *122*(9), 7267–7290. https://doi.org/10.1002/2017JC012952

Pierce, S. D., Smith, R. L., Kosro, P. M., Barth, J. A., & Wilson, C. D. (2000). Continuity of the poleward undercurrent along the eastern boundary of the mid-latitude north Pacific. *Deep Sea Research Part II: Topical Studies in Oceanography*, *47*(5–6), 811–829. ISSN 0967-0645. https://doi.org/10.1016/S0967-0645(99)00128-9

Pozo Buil, M., Jacox, M. G., Fiechter, J., Alexander, M. A., Bograd, S. J., Curchitser, E. N., et al. (2021). A dynamically downscaled ensemble of future projections for the California Current System. *Frontiers in Marine Science*, *8*. https://doi.org/10.3389/fmars.2021.612874

Ray, S., Siedlecki, S., Alexander, M. A., Bond, N. A., & Hermann, A. J. (2020). Drivers of subsurface temperature variability in the Northern California Current. *Journal of Geophysical Research: Oceans*, *125*(8), e2020JC016227. https://doi.org/10.1029/2020JC016227

Richaud, B., Kwon, Y.-O., Joyce, T. M., Fratantoni, P. S., & Lentz, S. J. (2016). Surface and bottom temperature and salinity climatology along the continental shelf off the Canadian and U.S. East Coasts. *Continental Shelf Research*, *124*, 165–181. https://doi.org/10.1016/j.csr.2016.06.005

Siedlecki, S. A., Kaplan, I. C., Hermann, A. J., Nguyen, T. T., Bond, N. A., Newton, J. A., et al. (2016). Experiments with Seasonal Forecasts of ocean conditions for the Northern region of the California Current upwelling system. *Scientific Reports*, *6*(1), 27203. https://doi.org/10.1038/srep27203

Slesinger, E., du Pontavice, H., Seibel, B., Saba, V. S., Kohut, J., & Saba, G. K. (2024). Climate-induced reduction in metabolically suitable habitat for U.S. northeast shelf marine species. *PLOS Climate*, *3*(4), e0000357. https://doi.org/10.1371/journal.pclm.0000357

Sulkin, S. D., Mojica, E., & McKeen, G. L. (1996). Elevated summer temperature effects on megalopal and early juvenile development in the Dungeness crab, Cancer magister. *Canadian Journal of Fisheries and Aquatic Sciences*, *53*(9), 2076–2079. https://doi.org/10.1139/f96-137

Szekely, T., Gourrion, J., Pouliquen, S., & Reverdin, G. (2019). CORA, Coriolis ocean dataset for reanalysis. *SEANOE*. https://doi.org/10.17882/46219

Szuwalski, C. S., Aydin, K., Fedewa, E. J., Garber- Yonts, B., & Litzow, M. A. (2023). The collapse of eastern Bering Sea snow crab. *Science*, *382*(6668), 306–310. https://doi.org/10.1126/science.adf6035

Thomson, R. E., & Krassovski, M. V. (2010). Poleward reach of the California Undercurrent extension. *Journal of Geophysical Research*, *115*(C9), C09027. https://doi.org/10.1029/2010JC006280

Uppala, S. M., Kållberg, P. W., Simmons, A. J., Andrae, U., Bechtold, V. D. C., Fiorino, M., et al. (2005). The ERA-40 re-analysis. *Quarterly Journal of the Royal Meteorological Society*, *131*(612), 2961–3012. https://doi.org/10.1256/qj.04.176

Veneziani, M., Edwards, C. A., Doyle, J. D., & Foley, D. (2009). A central California coastal ocean Modeling study: 1. Forward model and the influence of realistic versus climatological forcing. *Journal of Geophysical Research*, *114*(C4), C04015. https://doi.org/10.1029/2008JC004774

Wilks, D. S. (2020). Statistical methods in the atmospheric sciences, *fourth addition*. Elsevier. https://doi.org/10.1016/C2017-0-03921-6

Xu, T., Newman, M., Alexander, M. A., & Capotondi, A. (2024). Seasonal predictability of bottom temperatures along the North American West Coast. *Journal of Geophysical Research: Oceans*, *129*(9). accepted. https://doi.org/10.1029/2023jc020504